

UNIVERSITY OF CALGARY

Phase Equilibria of Hexane/Water and Hexane/Water/Bitumen Systems with Applications to  
Solvent-Aided Thermal Recovery Processes of Bitumen

by

Chukwuemeka Valentine Nwokoye

A THESIS

SUBMITTED TO THE FACULTY OF GRADUATE STUDIES  
IN PARTIAL FULFILLMENT OF THE REQUIREMENTS FOR THE  
DEGREE OF MASTER OF SCIENCE

GRADUATE PROGRAM IN CHEMICAL ENGINEERING

CALGARY, ALBERTA

JANUARY, 2023

© Chukwuemeka Valentine Nwokoye 2023

## **Abstract**

This thesis presents an experimental study of the phase equilibria of hexane/water and hexane/water/bitumen mixtures applicable to solvent-assisted thermal recovery processes. The solvent selection for solvent-aided thermal recovery processes is often chosen based on the proximity of solvent saturation properties to steam. In this thesis, such a premise is examined by evaluating the phase equilibria of hexane/water and hexane/water/bitumen mixtures to fill the existing knowledge gap and draw a conclusion on the validity of such a hypothesis.

First, a PVT setup was used to measure the vapor-liquid equilibria (VLE) of hexane/water binary mixtures at temperatures ranging from 183-215 °C and a constant pressure of 2.5 MPa. The results indicate an azeotropic behavior with a co-condensation temperature of 183.7 °C at a hexane mole-fraction of 0.6029. The Cubic Plus Association Equation of State (CPA-EoS) and activity coefficient-based Non-Random Two Liquid (NRTL) models were used to model the measured experimental data, and the predicted results are in good agreement with the measured data.

Next, the condensation properties of a solvent/water mixture in the presence of Mackay River Bitumen (ternary system) were performed. The phase behavior, viscosity, and density measurements were taken at two typical mole fractions of solvent (1 and 5%) in the steam/solvent mixture while keeping the hexane/bitumen ratio constant at temperatures ranging from 183-215 °C and a constant pressure of 2.5 MPa. The results revealed a vapor-liquid-liquid equilibrium (VLLE). The phases in equilibrium include a vapor phase consisting of hexane and water, a liquid phase comprising hexane/water bitumen, and a second liquid phase containing hexane/water. The condensation trends of the binary hexane/water and ternary hexane/water/bitumen systems were compared. The results revealed that the hexane concentration in the ternary systems is close to those of the binary mixture at any given temperature, suggesting that the binary system of solvent/water may be used for condensation

studies. In addition, the results revealed that the solubility of hexane in bitumen dominates viscosity reduction at the temperature range of interest. The cubic-plus-association equation of state (CPA EoS) was used to model the phase equilibria of hexane/water and hexane/water/bitumen mixtures. The findings provide insight into steam/solvent condensation behavior with applications to the solvent-aided thermal recovery of bitumen from oil sands.

## **Preface**

This thesis is an original work by the author. No part of this thesis has been previously published

## **Acknowledgement**

I would like to thank my supervisor, Dr. Hassan Hassanzadeh, for his trust in me by welcoming me to conduct my MSc research in the SHARP research consortium. I am grateful; your constructive feedback has made this a wonderful experience and learning curve.

I would like to express my heartfelt gratitude to Dr. Devjyoti Nath, who collaborated with me, provided guidance and technical support, and, most importantly, provided critical feedback that helped me learn. I am grateful for all your assistance with my research project.

I thank Mahmood Abdi for guiding me through the thermodynamic modeling process; I am grateful for your help.

I would like to thank all of the SHARP sponsors. They helped by providing the funding I needed to finish my project, including Canadian Natural Resource Limited, Cenovus Energy, CNOOC International, ConocoPhillips, Imperial Oil, Kuwait Oil Company, Strathcona Resources Limited, Suncor Energy, Mitacs, University of Calgary, Eyes High, and Schulich School of Engineering.

Finally, I would like to thank my family for supporting me and helping me finish my research project, especially my late father (whom I lost during my project time, I am sure you are proud of this achievement, and I wish you were here to celebrate this achievement with me). I want to express my gratitude for all the support to my friends and the lovely members of SHARP.

To all the late nights in the lab ...

## Table of Contents

Abstract	ii
Preface	iv
Acknowledgement	v
List of Figures	ix
List of Tables	x
List of Symbols, Abbreviations, and Nomenclatures	xi
Epigraph	xiii
Chapter One: Introduction	1
1-1 Overview	1
1-2 Research Objectives	3
1-3 Thesis structure	3
1-4 Reference	5
Chapter 2: Literature Review on the Solvent-Aided Thermal Recovery Process (SA-SAGD)	7
2-1 Concept of SA-SAGD	7
2-2 Numerical and Experimental Investigation into SA-SAGD Process	7
2-3 Experimental Phase Behavior and Thermophysical Data for Different Hydrocarbon Solvent and Bitumen	12
2-3-1 Methane-Bitumen	12
2-3-2 Ethane-Bitumen	13
2-3-3 Propane-Bitumen	14
2-3-4 Butane-Bitumen	15
2-3-5 Pentane-Bitumen	16
2-3-6 Hexane-Bitumen	17
2-3-7 Water-Bitumen	18
2-3-7 Water-Solvent	19
2-3-8 Water-Solvent-Bitumen	19
2-4 Reference	21
Chapter 3: Vapor-liquid Equilibria (VLE) of the binary mixture of normal hexane and water at $P = 2.5$ MPa and $T = (183.7-214.5$ °C)	28
3-1 Abstract	28
3-2 Introduction	28
3-3 Experimental	30
3-3-1 Material	30
3-3-2 Experimental Setup and Procedure	31
3-4 Verification of VLE measurements	35
3-5 Thermodynamic Modeling	36
3-5-1 Cubic Plus Association Equation of state (CPA-EoS) model	36
3-5-2 Non-Random Two Liquid (NRTL) model	38

3-5-3 Models' parameters and data correlation -----	38
3-6 Results and Discussion -----	39
3-7 Conclusion -----	45
3-8 References -----	46
Chapter 4: Experimental and modeling studies of phase behavior, viscosity, and density of normal-hexane, water, and Mackay River bitumen systems. -----	51
4-1 Abstract-----	51
4-2 Introduction -----	51
4-3 Experimental-----	56
4-3-1 Material -----	56
4-3-2 Experimental Setup-----	56
4-3-3 Procedure -----	58
4-4 Thermodynamic Modeling-----	61
4-4-1 Cubic Plus Association Equation of state (CPA-EoS) model -----	61
4-4-2 Models' parameters and data correlation -----	62
4-5 Results -----	63
4-5-1 VLLE Experiments of the ternary system of normal-hexane, water and Mackay River bitumen -----	63
4.5.2 VLLE modeling of the ternary system of normal-hexane, water and Mackay River bitumen-----	70
4-6 Summary and Conclusions -----	73
4-7 Reference-----	74
Chapter 5: Conclusions and Recommendations -----	78
5-1 Summary -----	78
5-2 Conclusion -----	78
5-3 Recommendation-----	79

## List of Figures

Figure 2-1: Experimental data range for Methane-Bitumen system.-----	13
Figure 2-2: Experimental data range for Ethane-Bitumen system.-----	14
Figure 2-3: Experimental data range for the Propane-Bitumen system.-----	15
Figure 2-4: Experimental data range for the Butane-Bitumen system.-----	16
Figure 2-5: Experimental data range for Pentane-Bitumen system.-----	17
Figure 2-6: Experimental data range for Hexane-Bitumen system.-----	18
Figure 3-1: Experimental setup for n-hexane-water VLE studies.-----	33
Figure 3-2: Liquid phase GC setup.-----	35
Figure 3-3: Measured composition of Methane ( $C_1$ ) in a binary mixture of Methane ( $C_1$ ) and n-Hexane ( $n-C_6$ ) at the temperatures of 75 °C and 100 °C was compared with the literature.	36
Figure 3-4: Vapor-liquid equilibria (T-xy) of n- $C_6$ / H <sub>2</sub> O binary system at ~2.5 MPa.-----	42
Figure 3-5: Comparison of the predicted liquid-liquid equilibria (T-xx) for n- $C_6$ /H <sub>2</sub> O binary system using NRTL model with the previously published data in literature at 0.1 MPa ( $\pm 0.01$ ).-----	43
Figure 4-1: Experimental setup for n-hexane-water-bitumen VLLE studies.-----	58
Figure 4-2: Liquid phase GC setup.-----	60
Figure 4-3: Comparison of the mole fraction of n- $C_6$ in the vapor phase of the ternary n- $C_6$ / H <sub>2</sub> O /Mackay River bitumen ternary system as compared with the n- $C_6$ / H <sub>2</sub> O binary system [20] at the range of studied temperatures and 2.5 MPa pressure.-----	65
Figure 4-4: Solubilities of n- $C_6$ and H <sub>2</sub> O in the oleic phase.-----	66
Figure 4-5: K value of n- $C_6$ with respect to the mole-fraction of n- $C_6$ in the hydrocarbon-rich oleic phase.-----	67
Figure 4-6: (a) Viscosity of the hydrocarbon-rich oleic phase. (b) Viscosity of the water-rich aqueous phase.-----	67
Figure 4-7: (a) The density of the hydrocarbon-rich oleic phase. (b) The density of the water-rich aqueous phase.-----	68
Figure 4-8: Solubilities of n- $C_6$ and H <sub>2</sub> O in the aqueous phase.-----	69

## List of Tables

Table 3-1: Specifications of materials. -----	30
Table 3-2: Parameters for CPA EoS for associating and non-associating components used in this study -----	39
Table 3-3: Experimental vapor-liquid equilibria (VLE) data (T, P, x, y) for the binary mixture of n-C <sub>6</sub> /H <sub>2</sub> O system. -----	40
Table 3-4: Regressed NRTL parameters for n-C <sub>6</sub> /H <sub>2</sub> O system. -----	43
Table 3-5: The activity coefficient of the n-C <sub>6</sub> and H <sub>2</sub> O. -----	44
Table 4-1: Specifications of materials. -----	56
Table 4-2: Model's parameter used in the VLE, LLE, and VLLE CPA EoS calculations. ----	63
Table 4-3: Phase behavior, viscosity, and density data for VLLE of the ternary n-C <sub>6</sub> /H <sub>2</sub> O/bitumen system. -----	71
Table 4-4 Cross-association and binary interaction parameters between water and bitumen pseudo-components [30]-----	72
Table 4-5: Bitumen parameters [30]-----	72
Table 4-6: Binary interaction parameters between n-C <sub>6</sub> and bitumen pseudo-components ---	72

## List of Symbols, Abbreviations, and Nomenclatures

2D	Two-dimensional
3D	Three-dimensional
bbf.	Barrel
BPR	Back pressure regulator
C <sub>1</sub>	Methane
C <sub>12</sub>	Dodecane
C <sub>2</sub>	Ethane
C <sub>3</sub>	Propane
C <sub>4</sub>	Butane
C <sub>5</sub>	Pentane
C <sub>7</sub>	Heptane
C <sub>8</sub>	Octane
CPA	Cubic Plus Association
EoS.	Equation of state
ES-SAGD	Expanding-solvent
FID	Flame ionization detector
GC	Gas Chromatography
LASER	Liquid Addition to Steam for Enhance Recovery
LLE	Liquid-liquid equilibria
m	Meter
mL	Millilitres
MPa	Mega Pascal

n-C <sub>6</sub>	Normal hexane
NCG	Non-condensable gas
NRTL	Non-random two-liquid
PVT	Pressure-Volume Temperature
RMSD	Root means square deviation
RS-SAGD	Rich-solvent SAGD
SA-SAGD	Solvent Assisted-SAGD
SAGD	Steam-assisted gravity drainage
SOR	Steam to oil ratio
T-xy	Temperature-mole fraction
TCD	Thermal conductivity detector
VLE	Vapor-liquid equilibria
VLLE	Vapor-liquid-liquid equilibria
Wt.	Weight

## **Epigraph**

What is dead may never die but rises again harder and stronger

■ George R.R. Martin, *A Song of Fire and Ice*

## **Chapter One: Introduction**

### **1-1 Overview**

The decline in conventional oil production, combined with an increase in global energy demand, has increased interest in heavy oil and bitumen production. Although Canada has one of the world's largest reserves (171 bbl), more than 97 % of these reserves (168 bbl) are in Alberta's oil sands [1]. Approximately 20 % of the oil sand deposits are within 75 m of the surface and viable for open-pit mining, while the remaining 80 % are deposited deeper than 75 m. Oil sand deposits greater than 75 m in depth necessitate special recovery techniques, and in-situ recovery offers a solution. The most common economically and fully developed viable in-situ method for bitumen recovery is steam-assisted gravity drainage (SAGD).

SAGD is a thermal in-situ bitumen recovery method where an injector well and a producer well are drilled horizontally and parallel to each other at the base of the oil sands formation, with the injector well approximately 5 m above the producer. Steam is injected through the injector well. The injected steam is condensed by transferring its latent heat to the bitumen, reducing the bitumen's viscosity. The mobilized oil then drains toward the production well by gravity [2]. The steam chamber expands and eventually reaches the top of the oil sands formation as the oil drains toward the production well. The vertical and horizontal expansion of the steam chamber results in heat losses to the overburden formation leading to high steam-oil-ratio (SOR). The SOR is the primary measure of the energy intensity for the SAGD process. A higher SOR indicates a less economical and environmentally friendly recovery process. The high volume of steam required per unit volume of the oil produced in the SAGD process is the main challenge, considering the energy requirements and the environmental impact [3]

Solvent co-injection with steam is being researched to lessen the high water need and energy intensity. Several in-situ recovery processes that involve the co-injection of solvents

with steam are currently being explored [4–10]. These processes include but are not limited to Solvent Assisted-SAGD (SA-SAGD)[11], N-SOLV [8], Enhanced Solvent Extraction Incorporating Electromagnetic Heating (ESEIEH) [10], and Liquid Addition to Steam for Enhance (LASER) [12]. Dissolution of solvent into the bitumen results in reduced viscosity and improved oil recovery. However, a poorly designed solvent process could lead to the loss of millions of dollars since solvent-aided methods have substantial capital and operating costs [13]. As a result, phase behavior, solubility, viscosity, and density measurements are crucial for modeling, simulating, and designing an optimized solvent-aided process.

The experimental phase behavior of steam and solvent co-condensation in the presence and absence of bitumen has not been reported in the literature. Previous studies have looked at vapor-liquid equilibria (VLE) and liquid-liquid equilibria (LLE) of solvent-bitumen, solvent/water, and water/bitumen systems and measured solvent-saturated bitumen's density, viscosity, solubility, and phase behavior. Although some LLE data for the n-C<sub>6</sub>/H<sub>2</sub>O binary system are previously reported in the literature, the experimental VLE, and VLLE data are scarce. Phase behavior study over a range of temperatures and mole fraction measurements at SA-SAGD operating pressure is necessary to understand the phase behavior of a solvent-steam co-injection. To the best of my knowledge, so far, no attempts have been made to perform a complete phase behavior study on the n-C<sub>6</sub>/H<sub>2</sub>O/Bitumen system applicable to SA-SAGD. The direct measurement and analysis of the VLE, LLE, and VLLE in the context of the steam-solvent co-condensation is challenging. A challenge in experimental VLE measurements of solvent/steam binary mixtures at pressure and temperatures of interest is the complex phase behavior of two immiscible liquids that can form a LL, VL, or VLLE at different operating conditions [14] and their low order of magnitude of mutual solubility [15]. These complexities highlight the importance of collecting experimental phase behavior measurements for the binary hydrocarbon solvent-steam mixtures to improve our understanding of such systems.

## **1-2 Research Objectives**

The primary goal of this study is to better understand the co-condensation of normal hexane (as a potential solvent for SA-SAGD) and water in the absence and presence of bitumen and acquire phase behavior and thermophysical property experimental data such as solubility, viscosity, and density at high temperatures and pressures for SA-SAGD application. To better understand the co-condensation characteristics of the n-C<sub>6</sub>/H<sub>2</sub>O mixture in a co-injection process, the VLE of the n-C<sub>6</sub>/H<sub>2</sub>O binary system was first explored. The experimental data acquired are modeled using the Cubic Plus Association (CPA) equation of state (EoS) and the Non-random two-liquid (NRTL) activity coefficient-based model to aid in the prediction of the phase behavior under various operating conditions. Next, n-C<sub>6</sub>/H<sub>2</sub>O co-condensation was studied in the presence of bitumen, and the corresponding thermophysical properties were measured. The effects of different n-C<sub>6</sub>/H<sub>2</sub>O and n-C<sub>6</sub>/bitumen ratios on the phase VLE were investigated. The measured experimental results are modeled using CPA EoS and NRTL models.

## **1-3 Thesis structure**

This thesis follows a research paper-based format and is structured into six chapters. Chapter 1 presents a brief introduction of the topic, a description of the research objective, and the thesis structure.

Chapter 2 presents a detailed literature review of the available numerical, simulation, and experimental data on solvent/bitumen, water/bitumen, and solvent/water systems.

Chapter 3 presents the vapor-liquid equilibria (VLE) of the binary mixture of normal hexane and water at  $P = 2.5$  MPa and  $T = (456.85-487.85$  K). The results of this chapter have been submitted for publication.

Chapter 4 presents the experimental measurement of the VLLE of the normal hexane/water/bitumen system at  $P = 2.5$  MPa and  $T = (456.85-487.85$  K). The measured viscosity and density of the saturated liquid phases are also reported in this chapter.

Chapter 5 concludes the general findings from this research study and presents the proposed future studies on solvent-water-bitumen systems.

#### **1-4 Reference**

- [1] Government of Canada, What are the oil sands?, (2020). <https://www.nrcan.gc.ca/our-natural-resources/energy-sources-distribution/fossil-fuels/crude-oil/what-are-oil-sands/18089>.
- [2] R.M. Butler, Thermal recovery of oil and bitumen, Old Tappan, NJ (United States); Prentice Hall Inc., United States, 1991. <https://www.osti.gov/biblio/5797813>.
- [3] H. Hassanzadeh, T. Harding, Analysis of conductive heat transfer during in-situ electrical heating of oil sands, Fuel. 178 (2016) 290–299. <https://doi.org/https://doi.org/10.1016/j.fuel.2016.03.070>.
- [4] M. Rabiei Faradonbeh, H. Hassanzadeh, T. Harding, Numerical simulations of bitumen recovery using solvent and water-assisted electrical heating, Fuel. 186 (2016) 68–81. <https://doi.org/https://doi.org/10.1016/j.fuel.2016.08.077>.
- [5] R.M Butler, I.J Mokrys, Solvent analog model of steam-assisted gravity drainage, AOSTRA J Res. 5 (1989) 17–32.
- [6] T.N. Nasr, G. Beaulieu, H. Golbeck, G. Heck, Novel Expanding Solvent-SAGD Process “ES-SAGD,” Journal of Canadian Petroleum Technology. 42 (2003). <https://doi.org/10.2118/03-01-TN>.
- [7] S. Gupta, S. Gittins, P. Picherack, Field Implementation of Solvent Aided Process, Journal of Canadian Petroleum Technology. 44 (2005). <https://doi.org/10.2118/05-11-TN1>.
- [8] J. Nenniger, E. Nenniger, Method and apparatus for stimulating heavy oil production, No. 6883607 B2, 2005.
- [9] A. Sadeghi, H. Hassanzadeh, T.G. Harding, B. MacFarlane, S. Bashti, P. Haghghat, Numerical modeling of electromagnetic-based thermal recovery techniques combined with solvent injection, Int J Heat Mass Transf. 151 (2020) 119393. <https://doi.org/https://doi.org/10.1016/j.ijheatmasstransfer.2020.119393>.

- [10] M. Trautman, D. Ehresman, N. Edmunds, G. Taylor, M. Cimolai, Effective Solvent Extraction System Incorporating Electromagnetic Heating, 20120118565 A1, 2013.
- [11] T.N. Nasr, G. Beaulieu, H. Golbeck, G. Heck, Novel expanding solvent-SAGD process “ES-SAGD,” *Journal of Canadian Petroleum Technology - J CAN PETROL TECHNOL.* 42 (2003).  
<https://doi.org/10.2118/03-01-TN>.
- [12] R. P. Leaute, Kathy E. Corry, Karl Pustanyk, Liquid addition to steam for enhancing recovery of cyclic steam stimulation or laser-CSS, 2,342,955, 2005.
- [13] A. Sadeghi, A. Boustani, H. Hassanzadeh, Optimization of the Operating Envelope of a Hot-Solvent Injection Process for Bitumen Recovery, *SPE Journal.* 27 (2022) 2268–2282.  
<https://doi.org/10.2118/209592-PA>.
- [14] M. Abdi, M. Zirrahi, H. Hassanzadeh, Vapor–Liquid–Liquid Equilibrium Modeling of Water/Bitumen/Solvent (C<sub>1</sub>, C<sub>2</sub>, C<sub>3</sub>, and n-C<sub>4</sub>) Mixtures Using a Cubic-Plus-Association Equation of State, *Ind Eng Chem Res.* 61 (2022) 8279–8292.  
<https://doi.org/10.1021/acs.iecr.2c00873>.
- [15] N. Haarmann, S. Enders, G. Sadowski, Modeling binary mixtures of n-alkanes and water using PC-SAFT, *Fluid Phase Equilib.* 470 (2018) 203–211.  
<https://doi.org/https://doi.org/10.1016/j.fluid.2017.11.015>.

## **Chapter 2: Literature Review on the Solvent-Aided Thermal Recovery Process (SA-SAGD)**

The main goal of this chapter is to present a detailed review of the work that has been done so far to understand solvent co-injection in the thermal recovery processes. This section provides a brief overview of the solvent-aided thermal recovery process (SA-SAGD) process, followed by a review of all works, including simulations, numerical, and experimental studies of solvents/bitumen, water/bitumen, and hexane/water systems presented.

### **2-1 Concept of SA-SAGD**

SA-SAGD process involves the co-injection of solvent and steam to improve bitumen production and reduce energy consumption. The selection of solvent is an essential step in the implementation of SA-SAGD processes [1]. The solvent is reported to condense with steam in the chamber during this process, and as a result, an optimal solvent used is thought to have similar saturation properties to steam [2]. In addition to the solvent type, the solubility of a solvent in bitumen is critical for the mass transfer that helps in viscosity reduction in SA-SAGD. Solvent solubility in thermal processes can be inferred by the solvent molecular weight (Orr 2009) [3], operating temperature, and pressure. A brief review of studies on the numerical and experimental investigation into the SA-SAGD process is presented in the following section according to the publication year.

### **2-2 Numerical and Experimental Investigation into SA-SAGD Process**

Ferguson et al. (2001) [4] conducted an experiment to investigate the effect of adding propane to steam as an additive to improve the recovery of 13.5 API oil from Venezuela's Morichal field. The experiment was carried out with different propane-to-steam injection ratios at 0.26 MPa and a steam injection temperature of 160 °C. According to the study's, injecting propane with steam improved recovery compared to injecting steam alone.

Nasr et al. (2003) [2] carried out a laboratory experiment in which they tested SA-SAGD in a cylindrical setup with eight hydrocarbon solvents ranging from C<sub>3</sub> to C<sub>8</sub> and diluent. The oil drainage rate was discovered to increase with increasing solvent carbon number until C<sub>6</sub> when it began to decrease.

The timing of the injection is an important factor to consider for an effective SA-SAGD process. For example, Gupta and Gittins (2006) [5] proposed an injection strategy for the Solvent Assisted Process (SAP), in which the butane is injected when the chamber reaches the reservoir's top. However, later, Jiang et al. (2012) [6] suggested that injecting solvent (C<sub>6</sub>) early in the process improved the oil rate but that injection should be stopped after a certain time. These results highlight the optimized operating conditions highly depend on the solvent type. In an in-situ bitumen recovery technique, Gates and Bunio (2006) [7] mixed hydrocarbon solvent with non-condensable gas (NCG). In the initial phase of the project, steam, solvent, and NCG were injected under high pressure, and then the injected fluids were changed to contain a high concentration of solvent and NCG and a lower amount of steam while still maintaining a warm steam chamber. The authors concluded that operating at a controlled pressure using an injection approach promoted solvent transfer into the depleted reservoir for viscosity reduction. Nasr and Ayodele (2006) [8], in a 2D experimental setup, studied the SA-SAGD using C<sub>4</sub>-C<sub>10</sub> on Cold Lake bitumen at high temperature and pressure. The process recovered up to 99% of the solvent, according to the results.

A simulation study was carried out by Boak and Palmgren (2007) [9] to investigate the effect of injecting single-component solvents, solvent mixtures, and naphtha. The study's findings indicated that naphtha reduced SOR and improved oil recovery when coinjected with steam.

Gates and Chakrabarty (2008) [10] developed a new injection strategy using a 3D heavy oil reservoir to optimize the SOR by considering the operating pressure and solvent-to-steam injection ratio.

Govind et al. (2008) [11] also investigated the effect of injecting different solvents (C<sub>4</sub> -C<sub>7</sub>) and solvent blends at a controlled solvent concentration using reservoir simulations. All solvents were reported to perform better than SAGD; however, at 4 MPa, butane outperformed other solvents.

Ayodele et al. (2009) [12] created a low-pressure SA-SAGD process to replace high-pressure SAGD in low-pressure Athabasca reservoirs. Five sets of experimental measurements were carried out with propane, and the results were based on recovery rate, recovery time, heat loss, steam chamber growth, and SOR. The authors concluded that low-pressure SA-SAGD could help recover untapped bitumen/heavy oils due to their low-pressure conditions.

Edmunds et al. (2009) [13] proposed using a general algorithm to optimize solvent injection rate and composition. Later, Peterson et al. (2010) [14] and Al-Gosayir et al. (2012) [15] used the proposed algorithms in their various studies.

Ayodele et al. (2010) [16] tested SA-SAGD with C<sub>6</sub> as the solvent using a 2D high-temperature and high-pressure experimental setup. They used CMG-STARs to history match the experimental data. Their SA-SAGD tests recovered 10.93 % more oil than SAGD.

In a 2D simulation study, Li and Mamora (2010a) [17] investigated the drainage mechanics of the solvent-assisted SAGD process using various hydrocarbon solvents up to C<sub>12</sub>. They demonstrated that the relative condensation of solvent and steam in bitumen results in vaporized solvent, liquid, and water films. They also concluded that injecting solvent at low concentrations resulted in better oil due to solvent solubility and heat transfer from the steam.

Li and Mamora (2010b) [18] investigated the SA-SAGD process using C<sub>7</sub> and xylene as solvents in a 2D experimental model. The authors concluded that adding solvent reduced bitumen viscosity but failed to keep the chamber temperature stable. They also mentioned that choosing an optimal solvent could help to shorten the condensation time.

Ardali et al. (2010) [19] investigated the feasibility of SA-SAGD in a 2D physical experimental model with C<sub>3</sub>, C<sub>4</sub>, C<sub>6</sub>, and C<sub>7</sub> as solvents. The experiment was carried out at 0.55 MPa, and solvent/steam co-injection was tested to optimize the critical variables involved in the SA-SAGD process on the Peace River bitumen. The optimal injected concentration was determined to be 10 %wt. of C<sub>4</sub>. On the other hand, the authors attributed the solvent performance to reservoir properties and operating conditions.

Al-Turki et al. (2010) [20] investigated the injection of NCG into low-pressure reservoirs with top water using the SA-SAGD. The investigation led the author to conclude that the addition of NCG aided in the reduction of heat loss from the top water zone. Deng et al. (2010) [21] used a 2D high-temperature and a high-pressure experimental setup to investigate the effectiveness of co-injecting solvent diluent alongside steam in SAGD. The lighter components of the diluent condensed in the steam chamber to improve bitumen production, whereas the heavier elements had no noticeable effect.

Akinboyewa et al. (2010) [22] investigated the optimal injection concentration of butane solvent in the SA-SAGD process using a numerical and simulation approach. The optimal solvent injection concentration was between 5 and 10%. Hosseini Mohebbati et al. [23] optimized the use of additives in conjunction with steam to produce three significant oil sand deposits (Athabasca, Cold Lake, and Lloydminster). The operating pressure was identified as a critical factor to consider during the optimization of the solvent process.

Ardali et al. (2012) [24] used a 2D cylindrical setup to compare the effect of co-injecting hexane and heptane with pure SAGD. Hexane was discovered to improve recovery compared to the standard SAGD method significantly. Lin et al. (2014) [25] investigated how permeability and drainage height affect the SA-SAGD process. The C<sub>5</sub> solvent was tested on a sand pack saturated with Lloydminster heavy oil, and the experiment was carried out in a

visual high-pressure physical model. A correlation was also developed to account for the effect of permeability and drainage height.

Perez-Perez et al. (2014) [26] used a sensitivity analysis to determine the optimal grid size for defining the near-edge steam chamber. Pure C<sub>4</sub> and C<sub>6</sub> solvents and blends were tested for the SA-SAGD on a 2D synthetic reservoir created with the STAR simulator's dynamic gridding features. The solvents tested performed well at various pressures, particularly C<sub>6</sub> at 2.5 and 3.5 MPa. Ghasemi and Whitson (2014) [27] numerically investigated the SA-SAGD process in an Athabasca 2D model. The effects of medium solvents (C<sub>5</sub>-C<sub>8</sub>) and heavy solvents (C<sub>15</sub>) on the oil-gas interface were studied. It was determined that the equilibrium k-values define the oil-gas interface.

Khaledi et al. (2015) [28] also investigated the optimal solvent and the effect of operating conditions on the performance of SA-SAGD experimentally and numerically. They concluded that the azeotropic state (phase behavior) influences solvent/steam condensation.

Keshavarz et al. (2015) [29] developed an optimal guideline for applying solvent steam conjecture by considering the oil production rate, solvent retention, and ultimate oil recovery. The multiphase binary solvent-steam mixture was used to describe temperature reduction in the chamber, and it was concluded that lighter solvents result in a more significant temperature reduction.

Abdi et al. (2022) [30] used the CPA EoS model to simulate the VLLE of a bitumen-water-solvent (C<sub>1</sub>, C<sub>2</sub>, C<sub>3</sub>, C<sub>4</sub>) systems. The tuned model presented a reasonable prediction of VLLE of solvent/water/bitumen CPA EoS and allowed predicting VLLE data based merely on binary VLE and LLE data.

Kumar et al. (2022) [31] conducted a simulation experiment to compare the effectiveness of SAGD and SA-SAGD on oil drainage in oil sands with shale barriers. As a result, C<sub>4</sub> SA-SAGD demonstrated more significant steam-solvent chamber expansion.

## **2-3 Experimental Phase Behavior and Thermophysical Data for Different Hydrocarbon**

### **Solvent and Bitumen**

Many mixture solubility studies on binary systems of solvent/bitumen and water/bitumen have been reported in the literature. A review of some of the solubility experimentally measured data in the open literature is presented in the following.

#### **2-3-1 Methane-Bitumen**

Svrcek and Mehrotra (1982) [32] presented experimental data on the solubility, viscosity, and density of methane-saturated Athabasca bitumen at temperatures ranging from 25 to 100 °C and pressures up to 10 MPa.

Fu et al. (1998) [33] measured the vapor-liquid equilibrium (VLE) of methane and Cold Lake bitumen systems at 70, 100, and 150 °C isotherms and pressures up to 10 MPa.

Zirrahi et al. (2017) [34] measured the phase behavior, viscosity, and density of light n-alkanes (C<sub>1</sub>- C<sub>4</sub>) and Mackay River bitumen at three temperatures (100,150,190 °C) and 4.7 MPa pressure. Methane has the most negligible solubility and viscosity reduction effect compared to the other solvents investigated. The authors successfully modeled methane solubility using Peng Robinson (PR) EoS, correlated viscosity using a mixing rule, and used a practical density approach to predict the density of the hydrocarbon-rich phase.

Nourozieh et al. (2016a) [35] measured the solubility, viscosity, and density of C<sub>1</sub>/Athabasca bitumen at various temperatures and pressures (up to 190 °C and 10 MPa). They reported that C<sub>1</sub> solubility in Athabasca bitumen is negligible at high temperatures compared to lower temperatures (i.e., 50 °C). As a result, the viscosity reduction magnitude is small at high temperatures with isotherms greater than 100 °C.

Haddadnia et al. (2018a) [36] studied the solubility, viscosity, and density of methane-saturated Athabasca bitumen at high temperatures of up to 260 °C and pressured up to 8 MPa. The measured experimental data were correlated using the PR EoS thermodynamic model. The

results showed that at a constant temperature, C<sub>1</sub> solubility increased with pressure, while temperature caused a decrease in bitumen viscosity at constant pressure. Figure 2-1 shows the experimental data range for the Methane-Bitumen system reported in the literature and among others. The P-T diagrams generated with NIST data are also plotted in Figure 2-1.

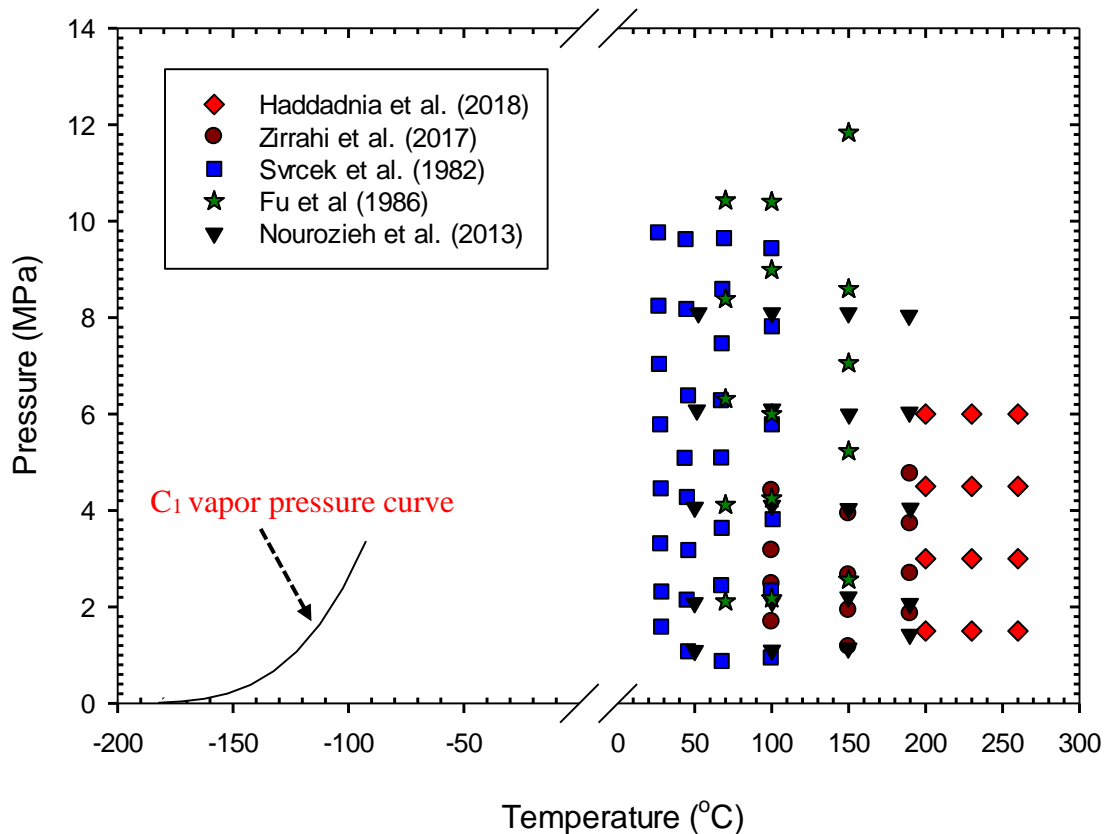


Figure 2-1: Experimental data range for Methane-Bitumen system.

### **2-3-2 Ethane-Bitumen**

Kariznovi et al. (2011) [37] reported the measured solubility, viscosity, and density of the C<sub>2</sub>/bitumen system at temperatures up to 190 °C and up to 10 MPa pressure. They discovered that C<sub>2</sub> solubility is negligible at temperatures above 150 °C, and a lower temperature results in significantly less viscosity reduction. Ganapathi et al. (2021) [38] used a microbalance to measure the solubility of C<sub>2</sub> in Lloydminster heavy oil at 17, 25, and 40 °C and pressures up to 2 MPa and modeled the measured data with PR-EoS.

The LLE of C<sub>2</sub>/Athabasca bitumen was studied by Nourozieh et al. (2011) [39] at room temperature and various pressures. Comparative research was done to see how the solvent-to-bitumen ratio affected the thermophysical properties. Viscosity was improved by raising the pressure or increasing the concentration ratio. Figure 2-2 shows some experimental data range for the ethane-bitumen system reported in the literature and among others. The P-T diagrams generated with NIST data are also plotted in Figure 2-2.

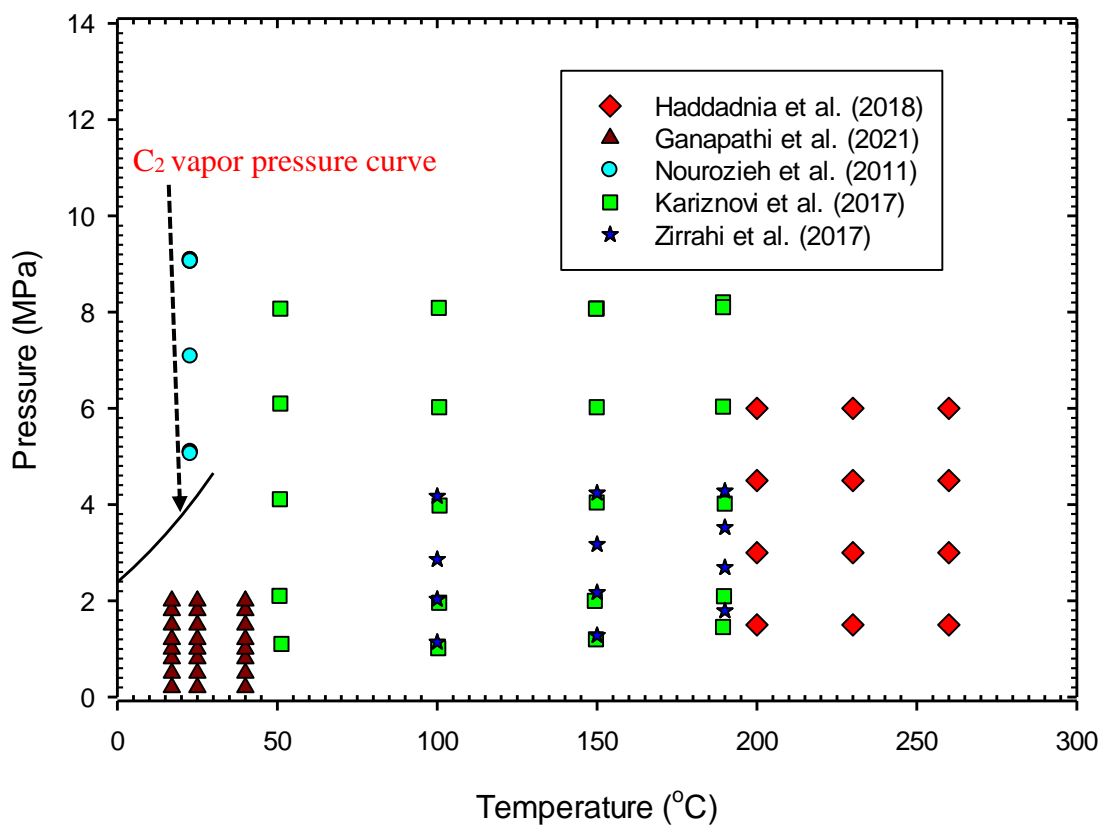


Figure 2-2: Experimental data range for Ethane-Bitumen system.

### 2-3-3 Propane-Bitumen

Nourozieh et al. (2015) [40] investigated the C<sub>3</sub>/Athabasca bitumen mixture under heated Vapex and SA-SAGD operating conditions at temperatures ranging from 50 to 200 °C and pressures up to 10 MPa. They observed a VLE and LLE at the investigated temperatures and pressures. At lower temperatures or/and higher pressures, the variation in C<sub>3</sub> solubility in

bitumen was significant. At higher experimental temperatures (200, 230, and 260 °C), Haddadnia et al. (2018) [36] observed a similar result. Figure 2-3 shows some experimental data range for the propane-bitumen system reported in the literature and among others. The P-T diagrams generated with NIST data are also plotted in Figure 2-3.

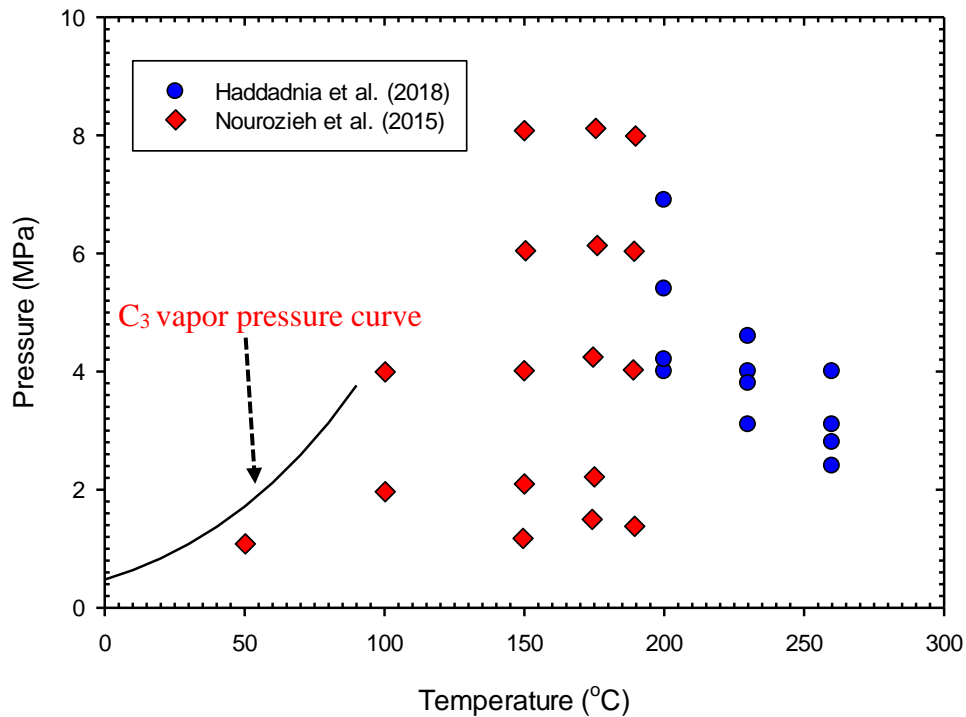


Figure 2-3: Experimental data range for the Propane-Bitumen system.

#### **2-3-4 Butane-Bitumen**

Nourozieh et al. (2016b) [41] measured the phase behavior, viscosity, and density of C<sub>4</sub>-saturated Athabasca bitumen at temperatures from 100 to 200 °C and pressures up to 6 MPa. C<sub>4</sub> has significantly affected bitumen viscosity at lower temperatures and higher pressures. Perez et al. (2019) [42] also investigated the phase behavior of bitumen extracted from Western Canadian reservoir and butane mixtures over a wide temperature and pressure range of up to 20 to 230 °C and 10 MPa, respectively. They reported single-phase liquid, VL, and LL equilibrium conditions at various temperatures and pressures. Furthermore, Haddadnia et al. (2018a) [36] measured the density and viscosity of butane- Athabasca bitumen mixtures at

higher temperatures, up to 260 °C. Figure 2-4 shows some experimental data range for the butane-bitumen system reported in the literature and among others. The P-T diagrams generated with NIST data are also plotted in Figure 2-4.

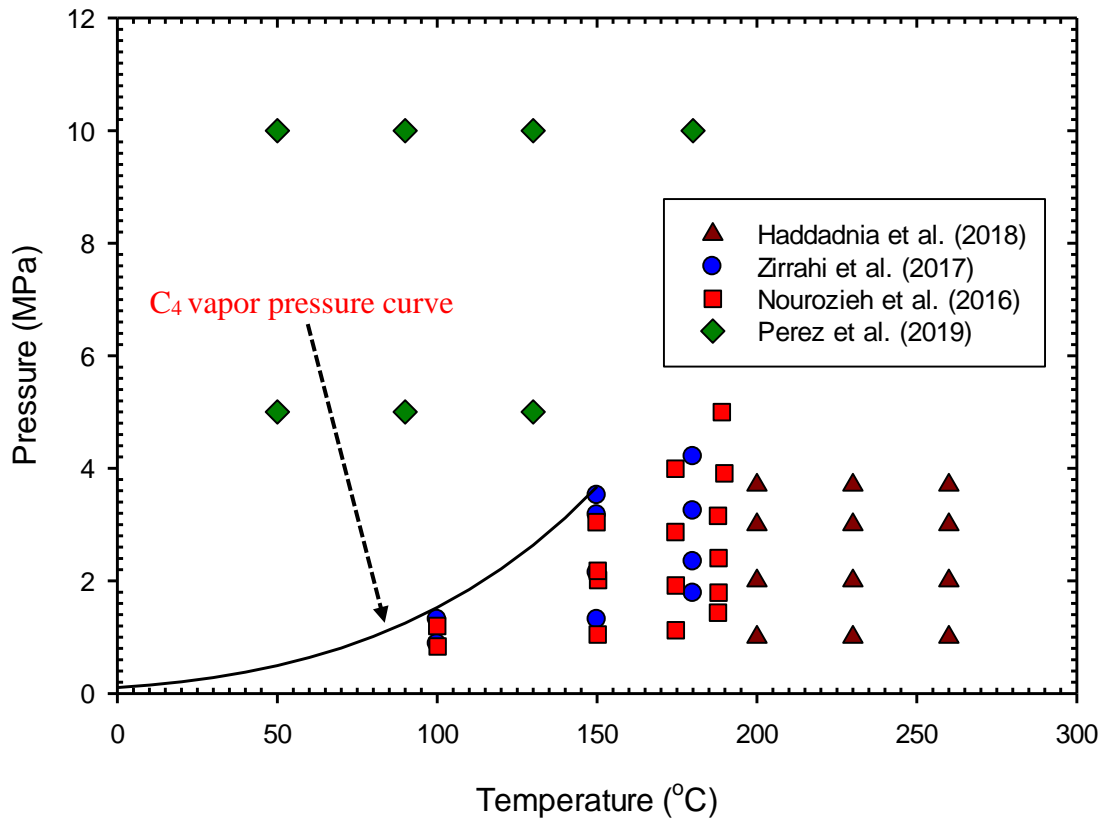


Figure 2-4: Experimental data range for the Butane-Bitumen system.

### 2-3-5 Pentane-Bitumen

Nourozieh et., (2014) [43] investigated the density of C<sub>5</sub>-saturated Athabasca bitumen at temperatures appropriate for in-situ processing and pipeline transportation. The experiment was carried out at various weight fractions of pentane and pressures of up to 10 MPa. Haddadnia et al. (2018b) [44] also studied the phase behavior viscosity and density of a C<sub>5</sub>/Athabasca bitumen system at temperatures ranging from 30-200 °C, pressures ranging from 2-8 MPa, and different concentrations. Figure 2-5 shows some experimental data range for the pentane-bitumen system reported in the literature and among others. The P-T diagrams generated with NIST data are also plotted in Figure 2-5

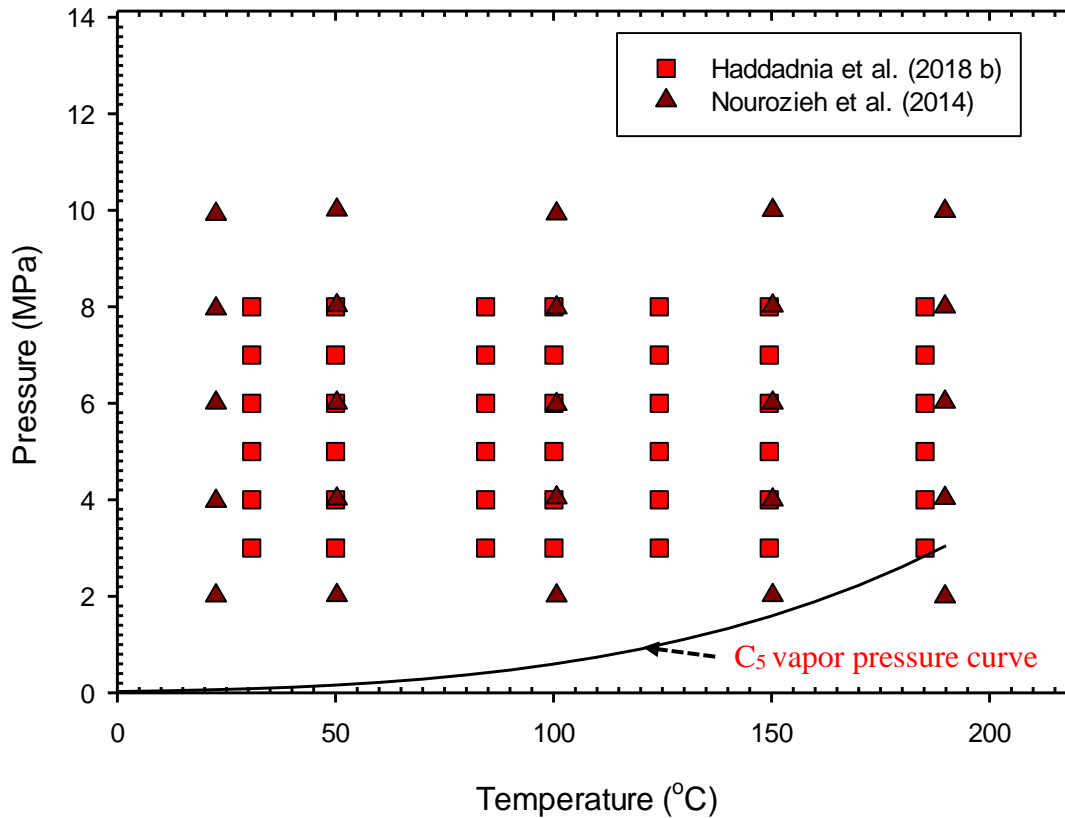


Figure 2-5: Experimental data range for Pentane-Bitumen system.

### 2-3-6 Hexane-Bitumen

Haddadnia et al. (2018b) [44] investigated the phase behavior, viscosity, and density of a C<sub>6</sub>/ Athabasca bitumen system at temperatures ranging from 30-200 °C, pressures ranging from 2-8 MPa, and different concentrations. According to the research, the density of bitumen decreases with increasing temperature and solvent concentration. The oil viscosity decreased with solvent concentration at a given temperature, but the effect of viscosity reduction due to solvent addition was generally reduced with increasing temperature. The viscosity of the mixture increased slightly as pressure was increased.

Gao et al. (2018) [45] also measured the phase behavior, viscosity, density, and asphaltene precipitation of C<sub>6</sub> and Athabasca bitumen mixtures at temperatures up to 160 °C and pressures up to 3 MPa. They reported that no liquid-liquid equilibrium was observed at the studied

conditions, even at high hexane concentrations (up to 90 wt.%) for the equilibrium mixtures. Figure 2-6 shows some experimental data range for the ethane-Bitumen system reported in the literature and among others. The P-T diagrams generated with NIST data are also plotted in Figure 2-6.

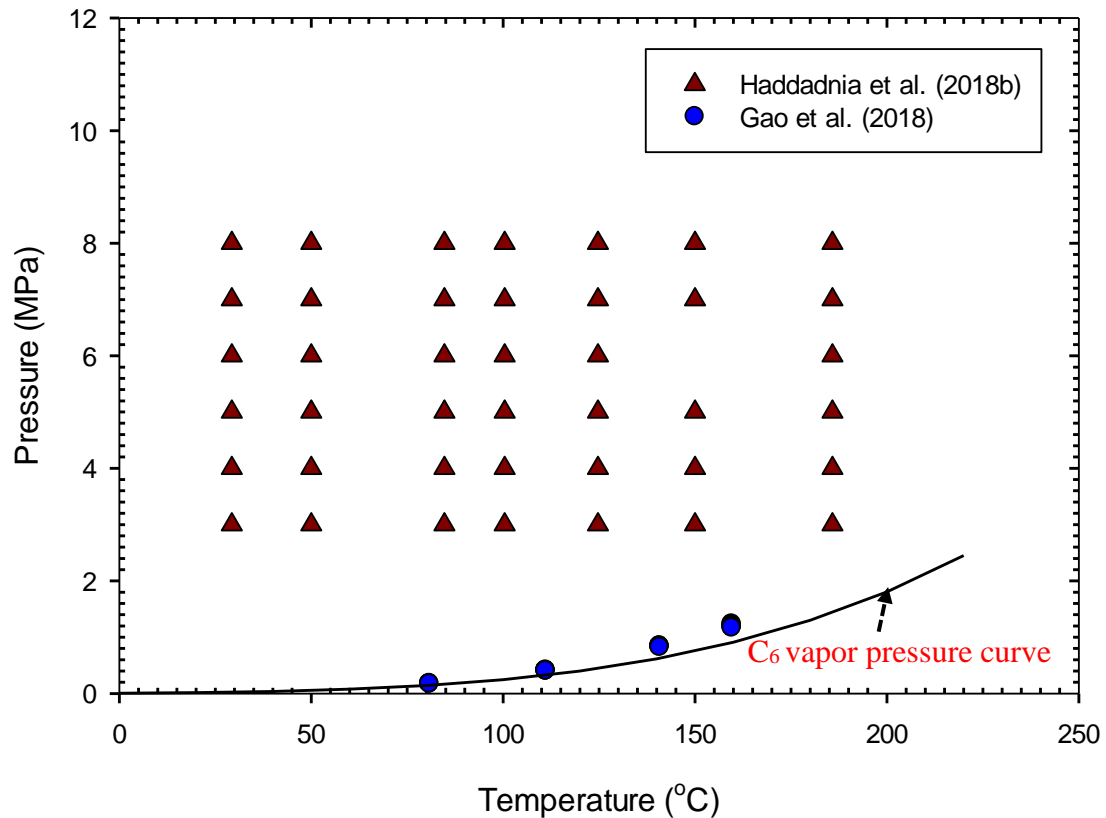


Figure 2-6: Experimental data range for Hexane-Bitumen system.

### 2-3-7 Water-Bitumen

Glandt and Chapman (1995) [46] investigated the effect of H<sub>2</sub>O dissolution on bitumen viscosity at high temperatures up to 290 °C with different gravity ranges ranging from 0.97 to 1.03 g/cm<sup>3</sup>. The measured water-saturated bitumen solubilities were compared with those from the mixing rule. They reported that the effect of temperature on water solubility in bitumen is more significant above 150 °C and that at 286 °C, the viscosity reduction was half of that

without water. The measured water solubility in bitumen samples differed from the predicted values of the mixing rule.

Amani et al. (2013) [47] also determined the water solubility of Athabasca bitumen over a temperature range relevant to the bitumen refining process (247-367 °C). According to the reported findings, water dissolution in bitumen follows an exponential increase with temperatures above 100 °C. Additionally, Zirrahi et al. (2017) [48] investigated water solubility in Mackay River bitumen at temperatures ranging from 100 to 220 °C and a pressure of 3.44 MPa. The water-saturated bitumen density and viscosity were also measured and correlated.

### **2-3-7 Water-Solvent**

Olds et al. (1942) [49] investigated the solubility of gas (C<sub>1</sub>) in water at high pressures up to 68 MPa and temperatures between 37- 237 °C. They observed a high variation in water concentration in the vapor phase at different operating conditions. Reamer et al. (1943) [50] studied experimentally the effect of pressure and temperature on the phase equilibrium of the C<sub>2</sub>/H<sub>2</sub>O system at similar temperatures and pressure investigated by Olds et al. [49]. The vapor phase trend at 104 °C was compared to similar systems of C<sub>1</sub>/H<sub>2</sub>O and Nitrogen (N<sub>2</sub>)/H<sub>2</sub>O at different pressures. Reamer et al. (1952) [51] also extended the previous work by measuring the phase equilibria of the C<sub>4</sub>/H<sub>2</sub>O mixture in the two-phase region. Kobayashi and Katz (1953) [52] reported the VLE data for C<sub>3</sub>/H<sub>2</sub>O mixtures at temperatures up to 149 °C. The reported fluid phase conditions were in the supercritical and VLE regions at the temperatures and pressures investigated.

### **2-3-8 Water-Solvent-Bitumen**

The ternary phase behavior data of a solvent-assisted thermal process is limited in the literature. Zirrahi et al. (2017) [34] measured the ternary phase behavior of such a system at temperatures up to 190 °C and pressures up to 5 MPa. The experiments were carried out with hydrocarbon solvents in the C<sub>1</sub>-C<sub>4</sub> range, and the measured solubility data were compared to

the same systems in the absence of water. The hydrocarbon-rich phase viscosity and density were also measured. Their studies did not include concentrations of the vapor phase or the water-rich phase. The studies also compared the ternary system to solvent/bitumen to compare the effect of water addition on solvent/bitumen phase behavior.

## **2-4 Reference**

- [1] N. Sabet, H. Hassanzadeh, J. Abedi, Selection of efficient solvent in solvent-aided thermal recovery of bitumen, *Chem Eng Sci.* 161 (2017) 198–205. <https://doi.org/https://doi.org/10.1016/j.ces.2016.12.031>.
- [2] T.N. Nasr, G. Heck, H. Golbeck, G. Beaulieu, Novel Expanding Solvent-SAGD Process “ES-SAGD,” *Journal of Canadian Petroleum Technology.* 42 (2003).
- [3] B. Orr, ES-SAGD; Past, Present and Future, in: Paper Presented at the SPE Annual Technical Conference and Exhibition, SPE, New Orleans, Louisiana, 2009. <https://doi.org/10.2118/129518-STU>.
- [4] M.A. Ferguson, D.D. Mamora, J.G. Goite, Steam-Propane Injection for Production Enhancement of Heavy Morichal Oil, in: 2001.
- [5] S.C. Gupta, S.D. Gittins, Christina Lake Solvent Aided Process Pilot, *Journal of Canadian Petroleum Technology.* 45 (2006).
- [6] H. Jiang, X. Deng, H. Huang, G. Beaulieu, G. Heck, O.G. Akinlade, T.N. Nasr, Study of solvent injection strategy in ES-SAGD process, Society of Petroleum Engineers, Calgary, AB, 2012. <https://doi.org/10.2118/157838-ms>.
- [7] I. Gates, G. Bunio, In Situ Process to Recover Heavy Oil and Bitume, US20080017372A1, 2006.
- [8] T. N Nasr, O. R Ayodele, New Hybrid Steam-Solvent Processes for the Recovery of Heavy Oil and Bitumen, in: Presented at the Abu Dhabi International Petroleum Exhibition and Conference, Abu Dhabi, 2006.
- [9] J. Boak, C. Palmgren, Preliminary Numerical Analysis for a Naphtha Co-injection Test During SAGD, *Journal of Canadian Petroleum Technology.* 46 (2007). <https://doi.org/10.2118/07-01-01>.

- [10] I.D. Gates, N. Chakrabarty, Design of the Steam and Solvent Injection Strategy in Expanding Solvent Steam-Assisted Gravity Drainage, *Journal of Canadian Petroleum Technology*. 47 (2008). <https://doi.org/10.2118/08-09-12-CS>.
- [11] P.A. Govind, S. Das, S. Srinivasan, T. Wheeler, Expanding solvent SAGD in heavy oil reservoirs, in: *International Thermal Operations and Heavy Oil Symposium*, SPE, Calgary, 2008.
- [12] O.R. Ayodele, T.N. Nasr, G. Beaulieu, G. Heck, Laboratory Experimental Testing and Development of an Efficient Low-Pressure ES-SAGD Process, in: *Paper Presented at the Canadian International Petroleum Conference*, Calgary, Alberta, 2009.
- [13] N. EDMUNDS, B. MOINI, J. PETERSON, Advanced Solvent-Additive Processes via Genetic Optimization, in: *Paper Presented at the Canadian International Petroleum Conference*, Calgary, Alberta, 2009.
- [14] J. Peterson, D. Riva, N.. Edmunds, S. Solanki, The Application of Solvent-Additive SAGD Processes in Reservoirs With Associated Basal Water, in: *Paper Presented at the Canadian Unconventional Resources and International Petroleum Conference*, SPE, Calgary, Alberta, Canada, 2010. <https://doi.org/10.2118/137833-MS>.
- [15] M. Algosayir, J. Leung, T. Babadagli, Design of Solvent-Assisted SAGD Processes in Heterogeneous Reservoirs Using Hybrid Optimization Techniques, *Journal of Canadian Petroleum Technology*. 51 (2011). <https://doi.org/10.2118/149010-MS>.
- [16] O.R. Ayodele, T.N. Nasr, J. Ivory, G. Beaulieu, G. Heck, Testing and history matching ES-SAGD (using hexane), *Society of Petroleum Engineers*, 2010. <https://doi.org/10.2523/134002-ms>.
- [17] W. Li, D.D. Mamora, Drainage Mechanism of Steam with Solvent Coinjection under Steam Assisted Gravity Drainage (SAGD) Process, in: *Presented at the International Oil*

- and Gas Conference and Exhibition in China, SPE, 2010.  
<https://doi.org/10.2118/130802-MS>.
- [18] W. Li, D.D. Mamora, Experimental Investigation of Solvent Co-Injection in Vapor and Liquid Phase To Enhance SAGD Performance, in: Paper Presented at the SPE Annual Technical Conference and Exhibition, SPE, Florence, Italy, 2010.  
<https://doi.org/10.2118/133277-MS>.
- [19] M. Ardali, M. Barrufet, Canadian Unconventional Resources & International Petroleum Conference, in: Paper Presented at Canadian Unconventional Resources & International Petroleum Conference, OnePetro, Calgary, 2010.
- [20] A.A. Alturki, I.D. Gates, B.B. Maini, Co-Injection of Noncondensable Gas Improves ES-SAGD Performance in Shallow Oil Sands Reservoirs With a Small Top Water Zone, in: Paper Presented at the Canadian Unconventional Resources and International Petroleum Conference, SPE, Calgary, Alberta, Canada, 2010.  
<https://doi.org/10.2118/137092-MS>.
- [21] X. Deng, H. Huang, L. Zhao, D.H.-S. Law, T.N. Nasr, Simulating the ES-SAGD Process With Solvent Mixture in Athabasca Reservoirs, *Journal of Canadian Petroleum Technology*. 49 (2010) 38–46. <https://doi.org/10.2118/132488-PA>.
- [22] J. Akinboyewa, S.K. Das, Y.-S. Wu, H. Kazemi, Simulation of Expanding Solvent – Steam Assisted Gravity Drainage in a Field Case Study of a Bitumen Oil Reservoir, in: Paper Presented at the SPE Improved Oil Recovery Symposium, SPE, Tulsa, Oklahoma, USA, 2010. <https://doi.org/10.2118/129963-MS>.
- [23] M.H. Mohebati, B.B. Maini, T.G. Harding, Optimization of Hydrocarbon Additives With Steam in SAGD for Three Major Canadian Oil Sands Deposits, in: Paper Presented at the Canadian Unconventional Resources and International Petroleum Conference, SPE, Calgary, Alberta, Canada, 2010. <https://doi.org/10.2118/138151-MS>.

- [24] M.. Ardali, M.. Barrufet, D.D. Mamora, Laboratory Testing of Addition of Solvents to Steam to Improve SAGD Process, in: Paper Presented at the SPE Heavy Oil Conference Canada, SPE, Calgary, Alberta, Canada, 2012. <https://doi.org/10.2118/146993-MS>.
- [25] L. Lin, H. Ma, F. Zeng, Y. Gu, Experimental and Numerical Studies of the Reservoir Permeability and Drainage Height Effects on the Solvent-Diluted Heavy Oil Gravity Drainage, in: Paper Presented at the SPE Heavy Oil Conference-Canada, SPE, Calgary, Alberta, Canada, 2014. <https://doi.org/10.2118/170096-MS>.
- [26] A.. Perez-Perez, M.. Mujica, I.. Bogdanov, J.. Hy-Billiot, A Methodological Analysis of the Mechanisms Associated to Steam-Solvent Co-Injection Processes Using Dynamic Gridding, in: Paper Presented at the SPE Improved Oil Recovery Symposium, SPE, Tulsa, Oklahoma, USA, 2014. <https://doi.org/10.2118/169075-MS>.
- [27] M. Ghasemi, C.H. Whitson, Numerical Investigation and Integrated Optimization of Solvent-SAGD Process, in: Paper Presented at the International Petroleum Technology Conference, IPTC, Kuala Lumpur, Malaysia, 2014. <https://doi.org/10.2523/IPTC-18033-MS>.
- [28] R. Khaledi, H. Motahhari, T. Boone, Optimized Solvent for Solvent Assisted-Steam Assisted Gravity Drainage (SA-SAGD) Recovery Process, in: Paper Presented at SPE Canada Heavy Oil Technical Conference, Calgary, n.d.
- [29] M. Keshavarz, R. Okuno, T. Babadagli, Optimal Application Conditions for Steam/Solvent Coinjection, SPE Reservoir Evaluation & Engineering. 18 (2015) 20–38. <https://doi.org/10.2118/165471-PA>.
- [30] M. Abdi, M. Zirrahi, H. Hassanzadeh, Vapor–Liquid–Liquid Equilibrium Modeling of Water/Bitumen/Solvent (C<sub>1</sub>, C<sub>2</sub>, C<sub>3</sub>, and n-C<sub>4</sub>) Mixtures Using a Cubic-Plus-Association Equation of State, Ind Eng Chem Res. 61 (2022) 8279–8292. <https://doi.org/10.1021/acs.iecr.2c00873>.

- [31] A. Kumar, H. Hassanzadeh, Impact of shale barriers on performance of SAGD and ES-SAGD — A review, *Fuel*. 289 (2021) 119850. <https://doi.org/https://doi.org/10.1016/j.fuel.2020.119850>.
- [32] W.Y. Svrcek, A.K. Mehrotra, Gas Solubility, Viscosity And Density Measurements For Athabasca Bitumen, *Journal of Canadian Petroleum Technology*. 21 (1982). <https://doi.org/10.2118/82-04-02>.
- [33] C.T. Fu, V.R. Puttagunta, G. Vilcsak, Gas Solubility Of Methane And Ethane In Cold Lake Bitumen At In Situ Conditions, *Journal of Canadian Petroleum Technology*. 27 (1988). <https://doi.org/10.2118/88-04-06>.
- [34] M. Zirrahi, H. Hassanzadeh, J. Abedi, Experimental and modeling studies of water, light n-alkanes and MacKay River bitumen ternary systems, *Fuel*. 196 (2017) 1–12. <https://doi.org/https://doi.org/10.1016/j.fuel.2017.01.078>.
- [35] H. Nourozieh, M. Kariznovi, J. Abedi, Measurement and Modeling of Solubility and Saturated-Liquid Density and Viscosity for Methane/Athabasca-Bitumen Mixtures, *SPE Journal*. 21 (2016) 180–189. <https://doi.org/10.2118/174558-PA>.
- [36] A. Haddadnia, H. Sadeghi Yamchi, M. Zirrahi, H. Hassanzadeh, J. Abedi, New Solubility and Viscosity Measurements for Methane–, Ethane–, Propane–, and Butane–Athabasca Bitumen Systems at High Temperatures up to 260 °C, *J Chem Eng Data*. 63 (2018) 3566–3571. <https://doi.org/10.1021/acs.jced.8b00443>.
- [37] M. Kariznovi, H. Nourozieh, J. Abedi, Vapor–Liquid Equilibrium of Bitumen–Ethane Mixtures for Three Athabasca Bitumen Samples, *J Chem Eng Data*. 62 (2017) 2198–2207. <https://doi.org/10.1021/acs.jced.7b00322>.
- [38] R. Ganapathi, A. Henni, E. Shirif, Solubility of carbon dioxide and ethane in Lloydminster heavy oil: Experimental study and modelling, *Can J Chem Eng*. 100 (2022) 1235–1243. <https://doi.org/https://doi.org/10.1002/cjce.24327>.

- [39] H. Nourozieh, M. Kariznovi, J. Abedi, Physical Properties and Extraction Measurements for the Athabasca Bitumen + Light Hydrocarbon System: Evaluation of the Pressure Effect, Solvent-to-Bitumen Ratio, and Solvent Type, *J Chem Eng Data*. 56 (2011) 4261–4267. <https://doi.org/10.1021/je2008846>.
- [40] H. Nourozieh, M. Kariznovi, J. Abedi, Experimental and modeling studies of phase behavior for propane/Athabasca bitumen mixtures, *Fluid Phase Equilib*. 397 (2015) 37–43. <https://doi.org/https://doi.org/10.1016/j.fluid.2015.03.047>.
- [41] H. Nourozieh, M. Kariznovi, J. Abedi, Solubility of n-Butane in Athabasca Bitumen and Saturated Densities and Viscosities at Temperatures Up to 200°C, *SPE Journal*. 22 (2016) 94–102. <https://doi.org/10.2118/180927-PA>.
- [42] Y.A. Perez Claro, F.F. Schoeggl, S.D. Taylor, H.W. Yarranton, Phase Behavior of Mixtures of Bitumen and n-Butane, *Energy & Fuels*. 33 (2019) 8530–8543. <https://doi.org/10.1021/acs.energyfuels.9b02113>.
- [43] H. Nourozieh, M. Kariznovi, J. Abedi, Measurement and Prediction of Density for the Mixture of Athabasca Bitumen and Pentane at Temperatures up to 200 °C, *Energy & Fuels*. 28 (2014) 2874–2885. <https://doi.org/10.1021/ef4022784>.
- [44] A. Haddadnia, M. Zirrahi, H. Hassanzadeh, J. Abedi, Thermo-Physical Properties of n-Pentane/Bitumen and n-Hexane/Bitumen Mixtures Systems, *Can J Chem Eng*. 96 (2017). <https://doi.org/10.1002/cjce.22873>.
- [45] J. Gao, R. Okuno, H.A. Li, A Phase-Behavior Study for n-Hexane/Bitumen and n-Octane/Bitumen Mixtures, *SPE Journal*. 23 (2017) 128–144. <https://doi.org/10.2118/186097-PA>.
- [46] C.A. Glandt, W.G. Chapman, Effect of Water Dissolution on Oil Viscosity, *SPE Reservoir Engineering*. 10 (1995) 59–64. <https://doi.org/10.2118/24631-PA>.

- [47] M.J. Amani, M.R. Gray, J.M. Shaw, Volume of mixing and solubility of water in Athabasca bitumen at high temperature and pressure, *Fluid Phase Equilib.* 358 (2013) 203–211. <https://doi.org/10.1016/j.fluid.2013.07.021>.
- [48] M. Zirrahi, H. Hassanzadeh, J. Abedi, Experimental and modeling studies of MacKay River bitumen and water, *J Pet Sci Eng.* 151 (2017) 305–310. <https://doi.org/10.1016/j.petrol.2017.01.013>.
- [49] R.H. Olds, B.H. Sage, W.N. Lacey, Phase Equilibria in Hydrocarbon Systems. Composition of the Dew-Point Gas of the Methane-Water System, *Ind Eng Chem.* 34 (1942) 1223–1227. <https://doi.org/10.1021/ie50394a018>.
- [50] H.H. Reamer, R.H. Olds, B.H. Sage, W.N. Lacey, Phase Equilibria in Hydrocarbon Systems. Composition of Dew-Point Gas in Ethane-Water System, *Ind Eng Chem.* 35 (1943) 790–793. <https://doi.org/10.1021/ie50403a012>.
- [51] H.H. Reamer, B.H. Sage, W.N. Lacey, Phase Equilibria in Hydrocarbon Systems. n-Butane-Water System in the Two-Phase Region., *Ind Eng Chem.* 44 (1952) 609–615. <https://doi.org/10.1021/ie50507a049>.
- [52] R. Kobayashi, D. Katz, Vapor-Liquid Equilibria For Binary Hydrocarbon-Water Systems Correlation of Data, *Ind Eng Chem.* 45 (1953) 446–451. <https://doi.org/10.1021/ie50518a052>.

## **Chapter 3: Vapor-liquid Equilibria (VLE) of the binary mixture of normal hexane and water at P = 2.5 MPa and T= (183.7-214.5 °C)**

### **3-1 Abstract**

The vapor-liquid equilibria (VLE) of the binary mixture of the n-C<sub>6</sub>/H<sub>2</sub>O system at P=2.5 MPa and T= (183.7-214.7 °C) were reported in this study. The result showed an azeotropic behavior with a co-condensation temperature of 183.7 °C at an n-C<sub>6</sub> mole fraction of 0.6029. The measured experimental data were modeled with the Cubic Plus Association Equation of State (CPA-EoS) and activity coefficient-based Non-Random Two Liquid (NRTL) model. The infinite dilution activity coefficient of n-C<sub>6</sub> and H<sub>2</sub>O were also estimated over the temperature range of interest. The overall root means square deviation (RMSD) of the n-C<sub>6</sub> mole-fraction in vapor and liquid phases for the CPA EoS model was 0.0234, and those of the NRTL model were 0.0765.

**Keywords:** Vapor-liquid equilibrium; azeotropic behavior; CPA-EoS; NRTL; co-condensation; hexane/water system

### **3-2 Introduction**

There is a great interest in studying the VLE of the binary mixtures of n-alkane-water systems in various hydrocarbon processing operations [1–3]. Furthermore, hexane is recently considered a diluent for SA-SAGD for in-situ bitumen extraction from oil sands. Co-injection of hydrocarbon solvents with steam has increasingly gained popularity due to high solubility in bitumen, reducing the viscosity of bitumen and SOR, thus reducing the energy intensity of bitumen recovery processes. Accurately measured thermodynamic properties are essential to understanding the co-condensation behavior of the solvent-steam mixtures (i.e., n-C<sub>6</sub> and H<sub>2</sub>O). Solvent-steam co-injection processes are reported under various commercial names, including expanding-solvent SAGD (ES-SAGD) [4], rich-solvent SAGD (RS-SAGD) [5], and solvent-aided SAGD (SA-SAGD) [6]. The concept behind solvent-steam co-injection is the ability of

the solvent to reduce bitumen viscosity simultaneously, leading to improved bitumen drainage toward production wells at a lower energy cost. Mass transfer occurs through solvent dilution into the bitumen, decreasing bitumen viscosity more than what would have been achieved by heating with steam alone at a lower temperature [7]. For this phenomenon to occur, a solvent-steam mixture must be maintained in a vapor phase until the mixture approaches the viscous oil, where co-condensation takes place [8]. A challenge in experimental VLE measurements of solvent-steam systems at pressure and temperatures of interest is the complex phase behavior of two immiscible liquids that can form a LL and VL at different operating conditions [9] and their low order of magnitude of mutual solubility [1]. These complexities highlight the importance of collecting experimental phase behavior measurements for the binary hydrocarbon solvent-steam mixtures to improve our understanding of such systems.

A common assumption in selecting the optimum solvent for in-situ bitumen recovery has been the proximity of the solvent vaporization temperature to steam. Normal hexane (n-C<sub>6</sub>) has the closest vaporization temperature (221.33 °C) to steam (223.95 °C) at 2.5 MPa. As such, our work focuses on the VLE measurement and modeling of the hexane-steam system under SA-SAGD operating conditions. This study provides the first VLE experimental data on n-C<sub>6</sub>/H<sub>2</sub>O at P = 2.5 MPa and T=(183.7-214.7 °C). The noted pressure and temperature range are of interest in solvent-aided bitumen recovery processes. Although liquid-liquid phase equilibria data for the n-C<sub>6</sub>/H<sub>2</sub>O binary system are previously reported in the literature [10–16], experimental vapor-liquid phase equilibria data are very limited. Most of the previous studies focused on the near and supercritical regions at high temperatures and pressures, and they also reported PT data of the three-phase lines for different compositions of the n-C<sub>6</sub>/H<sub>2</sub>O binary system [17–20]. Barrufet et al. [21] reported five TPxy data points over a range of temperatures and pressure of 99.96-190.52 °C and 0.343-2.956 MPa, respectively. However, to understand such a binary system for solvent-steam co-injection, the temperature and mole

fraction measurements at constant pressure are necessary to capture the co-condensation of steam and n-C<sub>6</sub>. The model predicted VLE (T-xy) data were previously reported with the co-condensation temperature of 173.1 °C at 0.575-mole fraction of n-C<sub>6</sub> at 2.0 MPa [22] and 182 °C at 0.64-mole fraction of n-C<sub>6</sub> at 2.5 MPa [6].

This chapter presents an experimentally measured phase diagram of n-C<sub>6</sub>-H<sub>2</sub>O at an operating pressure of 2.5 MPa and a temperature range of 183.7-214.7 °C. Equilibrium conditions were attained in a high-pressure/high-temperature PVT cell. Equilibrium samples were analyzed with gas chromatography (GC), and the VLE results were used to generate a temperature-mole fraction (T-xy) diagram of the n-C<sub>6</sub>-H<sub>2</sub>O system. Due to the lack of experimental data on the desired system, the experimental setup was validated with a methane-n-hexane (CH<sub>4</sub> /n-C<sub>6</sub>) binary system. Experimental data were modeled using the cubic plus association equation of state (CPA EoS) and the activity coefficient-based Non-Random Two Liquid (NRTL) model.

### **3-3 Experimental**

#### **3-3-1 Material**

IUPAC systematic names, CAS registry number, supplier, and purity of the chemicals and gas used in this study are listed in Table 3-1. All the chemicals used in this study required no further purification; however, DI water prepared in the lab was boiled and degassed using a sonicator before using in this study.

Table 3-1: Specifications of materials.

<b>IUPAC systematic name</b>	<b>CAS Registry Number</b>	<b>Supplier</b>	<b>Purity <sup>a,b</sup> (%)</b>
Helium	CAS 7440-59-7	Linde Canada	99.999 mol%
Methane	CAS 74-82-8	Linde Canada	99.99 mol%
Ethane	CAS 74-84-0	Linde Canada	99.00 wt%
n-hexane	CAS 110-54-3	VWR	97.00 wt%
DI Water	CAS 7732-18-5	Prepared in Lab	-

<sup>a</sup> Purity data was provided by the supplier.  
<sup>b</sup> The provided chemicals were used directly in the experiments without further purification.

### **3-3-2 Experimental Setup and Procedure**

The experimental setup used to study the VLE of the n-hexane and water binary mixture is shown in Figure 3-1. The major component of this setup includes a Blue M oven, an Equilibrium PVT cell, a Visual Cell, a Gas Chromatography (GC), and a Quizix pump. The PVT cells used for the study contained a piston sealed by two O-rings used for isolating the liquid present at the top of the piston from the hydraulic fluid underneath. These O-rings are compatible with operating conditions and chemicals. The maximum internal volume of the PVT cell used for the VLE study was 2,200 ml; the cell's volume and pressure were controlled using a Quizix pump by injecting or receiving the hydraulic fluid from underneath the piston with a displacement accuracy of 0.002 ml. The injected or received hydraulic fluid enabled the piston's upward and downward movement, which controlled the internal cell volume until equilibration was reached. For faster and proper mixing, the PVT cell was designed to have a rocking system by placing a metal ball inside the cell that caused agitation of the mixtures. The Blue M oven attained and maintained the required equilibrium temperatures (the actual system temperature was recorded with an external RTD probe). The entire experimental setup was adequately cleaned before every VLE experiment, and then the piston was carefully placed inside the cell to eliminate trapped air underneath the piston.

For loading the water and n-hexane, the piston inside the PVT cell was placed at the top all the way, and Valve V-4 and V-2 were closed. Hence, water (from cell 13) was charged through the tube until the water came out through the waste line via valve V-3 to fill the line completely with water. Pressurized air was used to compress the water in cell 13. When the tube was filled with water, valve V-3 was closed, and valve V-2 was opened to charge water into the PVT cell. Then required amount of hydraulic fluid was received from underneath the piston using a Quizix pump, and the same amount of water was transferred at the top of the piston since the water was compressed. When the transfer of water was completed, valve V-2

was closed. Then valve V-3 was opened and vacuumed the tube via the waste line. Next, the tube was filled with hexane, similar to water. Hence, valve V-2 was opened, and the required amount of n-hexane was transferred to the PVT cell in a similar process of water transfer. Since hexane is compressible and water is almost incompressible, water was transferred at first. The actual mole of hexane and water was estimated using the exact density data of that actual operating condition. Then the valve (V-2) at the top of the VLE cell was closed after sample injection. The required mass and volume of the injected liquid were estimated with the density at the injection pressure. Afterward, the Blue M oven was operated at the desired temperature. Then the Quizix pump was set on “paired constant pressure bi-directional” operating mode to maintain the desired pressure of the PVT cell by either receiving or delivering the hydraulic liquid underneath the piston. The cell was rocked for more than 25 hours until the system reached equilibrium. Stability in the pump’s cumulative volume being shown on the computer indicated the system equilibrium. When the system was at equilibrium, the cell was kept in a vertical position for approximately four hours to allow the phases separate by the difference in their densities. Hence, the back-pressure regulator (BPR) was set at the VLE system pressure, and all the lines were vacuumed and pressurized with helium at the same VLE system pressure. Helium, an inert gas, was selected as it also served as the carrier gas for gas chromatography. Then the V-2 valve was opened, and the Quizix pump was set on “paired constant flow delivery” operating mode at a low flow rate (~ 4 ml/min) to move the piston upward and displace the equilibrium samples to the top of the piston through the V-2 valve. Displaced equilibrium samples were sequentially passed through the tube, visual cell, and BPR. The visual cell was placed before the BPR to monitor the gas and liquid phase samples. BPR positioned at the top of the visual cell maintained the system pressure at desired VLE system pressure. The three-way valve placed after the BPR allowed the gas phase samples to ass

through the packed bed (4) (packed with small stainless-steel balls for perfect mixing) and the liquid phase sample to move toward the Liquid Waste.

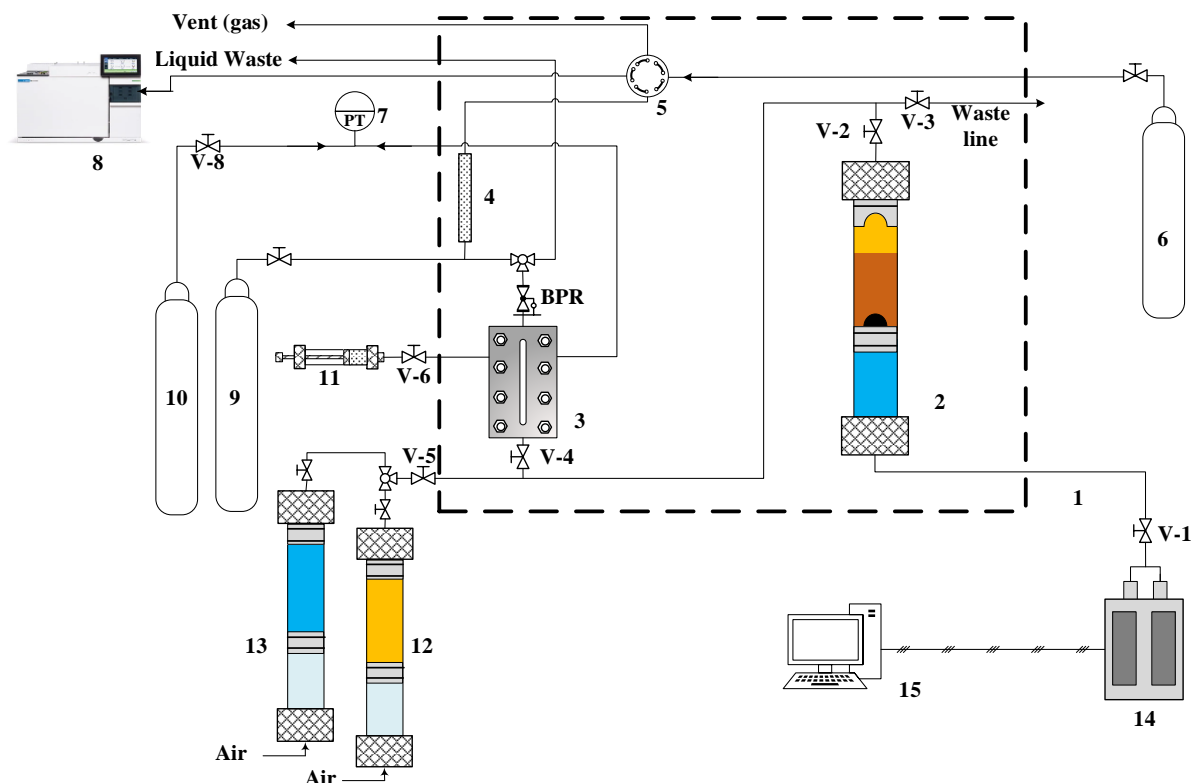


Figure 3-1: Experimental setup for n-hexane-water VLE studies. (1) Blue M oven, (2) Equilibrium cell, (3) Visual Cell, (4) Packed bed, (5) Ten-port valves, (6) Helium cylinder (Carrier Gas), (7) Pressure gauge, (8) Gas Chromatography (GC), (9) Gas Mixture cylinder (Ethane/Helium), (10) Helium cylinder, (11) liquid sample collector cell, (12) Distilled water feed cell, (13) n-Hexane feed cell, (14) Quizix pump, and (15) Computer.

Gas-phase and liquid-phase samples were analyzed with gas chromatography (GC). GC 8890 (Agilent Technologies) and GC-2010 (Shimadzu) were used to analyze the gas and liquid phase samples. Both GC systems were equipped with two injectors, two separate columns, and two detectors (thermal conductivity detector (TCD) and flame ionization detector (FID)). TCD detector was used to detect the water and ethane, and FID was used to detect all the hydrocarbons in the mixture. Gas-phase equilibrium samples were placed at the top of the

liquid phase samples due to the lower density; therefore, the gas phase sample was first passed through the BPR, followed by the liquid phase sample. The escaped gas phase sample from the BPR was moved through the three-way valve, mixed with an ethane-helium gas mixture, and passed through the pack-bed for perfect mixing. The final gas mixture was transferred towards the Vent (gas) through a Ten-port valve (5). A particular volume of gas-phase samples was sent to the TCD and FID GC systems at frequent intervals using the Ten-port valve for analyses. When all the gas-phase samples were passed through the BPR, liquid phase samples were moved toward the Liquid Waste through the three-way valve. Hence, two to three liquid phase samples were taken using liquid sample collector cells (11) through valve V-6 for GC analyses.

A separate experimental setup was used to analyze the liquid phase sample (shown in Figure 3-2). At first, liquid samples were charged through valve V-1 in equilibrium cell (2), and the valve was closed. Then a small amount of high-pressure ethane was charged from the ethane cell (5) to push the entire liquid sample inside the Equilibrium cell (2). The temperature of the equilibrium cell was maintained at 180 °C in an Oven. Sufficient time was provided for the complete evaporation of the liquid sample and the formation of a homogeneous mixture of C<sub>2</sub>/C<sub>6</sub>/H<sub>2</sub>O. Then the homogeneous mixture was moved toward the gas sample outpost through a Ten-port valve. A specific volume of the homogeneous gas mixture was sent to the GC using the Ten-port valve for analysis.

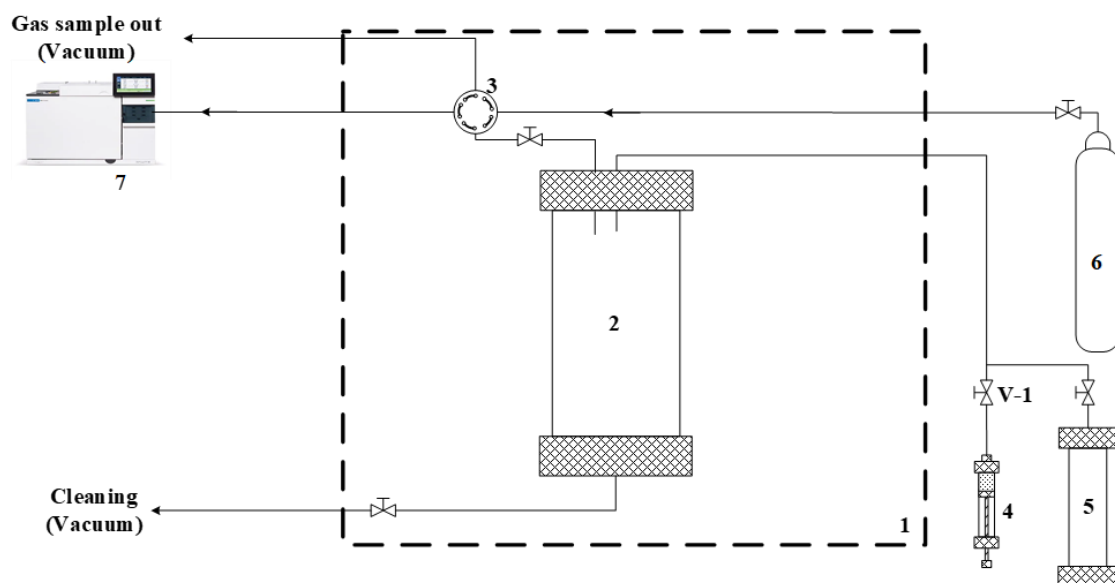


Figure 3-2: Liquid phase GC setup. (1) Blue M oven, (2) Equilibrium cell, (3) Ten-port valve, (4) Collector cell, (5) Ethane, (6) Helium, and (7) GC.

### **3-4 Verification of VLE measurements**

Vapor-liquid equilibrium studies for methane ( $\text{CH}_4$ ) and n-Hexane ( $\text{n-C}_6$ ) binary systems were performed at  $75\text{ }^\circ\text{C}$  and  $100\text{ }^\circ\text{C}$ . The compositions of  $\text{CH}_4$  and  $\text{n-C}_6$  in gas and liquid phases were measured multiple times with Gas-chromatography (GC) analysis, and the average compositions measured with GC at each temperature were compared with literature data [23–26]. The comparison among the results of this study and the literature is shown in Figure 3-3. It infers that the VLE studies were found to be in good agreement with the previously published literature.

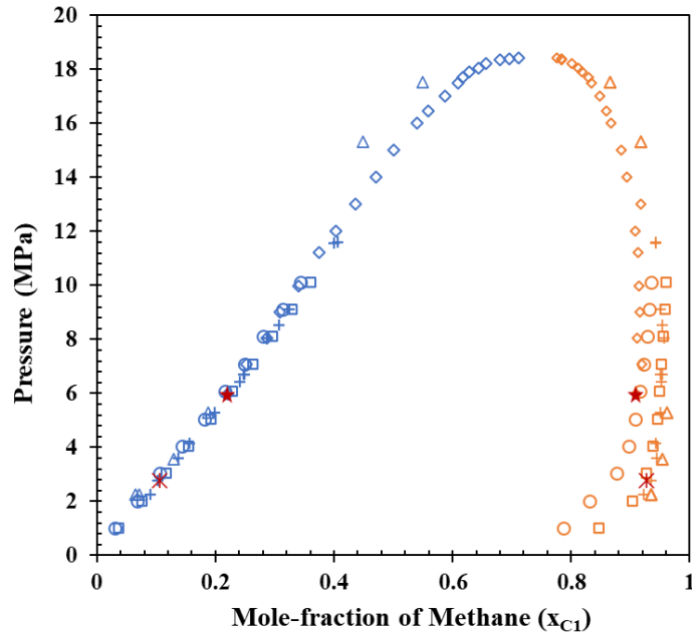


Figure 3-3: Measured composition of Methane ( $C_1$ ) in a binary mixture of Methane ( $C_1$ ) and n-Hexane ( $n-C_6$ ) at the temperatures of 75 °C and 100 °C was compared with the literature.

This study: \*, Run 1 at 75 °C and 2.79 MPa; and \*, Run 2 at 100 °C and 5.98 MPa. Literature: ○, Shim et al. at 99.74 °C; ◇ [23], Marteau et al. at 99.85 °C [26]; □, Shim et al. at 74.97 °C [23]; △, Cebola et al. at 75 °C [24]; and +, Chylinski et al. at 75 °C [25].

### **3-5 Thermodynamic Modeling**

Experimental VLE data for the n-Hexane ( $n-C_6$ ) and water ( $H_2O$ ) binary systems were correlated with the Cubic Plus Association Equation of State (CPA-EoS) and activity coefficient-based Non-Random Two-Liquid (NRTL) model.

#### **3-5-1 Cubic Plus Association Equation of state (CPA-EoS) model**

CPA is an equation of state model (EoS) that combines the cubic SRK EoS model with an advanced association term based on Wertheim's theory to properly explain the polar/association effects of the pure component or mixture [27], and this model reduces to the SRK EoS model when no association is present. CPA EoS can be expressed as the pressure term using the simplified equation [28] depicted in Eq. (1).

$$P = \frac{RT}{V_m - b} - \frac{a(T)}{V_m(V_m + b)} - \frac{1}{2} \frac{RT}{V_m} \left( 1 + \rho_m \frac{\partial \ln g}{\partial \rho_m} \right) \sum_i z_i \sum_{A_i} (1 - X_{A_i}) \quad (3-1)$$

where,  $P$ ,  $T$ ,  $R$ ,  $V_m$  and  $\rho_m$  are the pressure, temperature, universal gas constant, molar volume, and molar phase density, respectively.  $a(T)$  and  $b$  are the energy and co-volume parameters, respectively, which are estimated using SRK EoS [29]. The parameter  $X_{A_i}$  represents the mole-fraction of site A on molecule  $i$  that is not associated with other association sites as shown in Eq. (2) in terms of association parameter, and this term is used for estimating the self-association and cross-association of the component  $i$ .

$$X_{A_i} = \frac{1}{1 + \rho_m \sum_j z_j \sum_{B_j} X_{B_j} \Delta^{A_i, B_j}} \quad (3-2)$$

where the parameter  $Z_j$  is the mole-fraction of molecule  $j$ ,  $\Delta^{A_i, B_j}$  is the association strength between site A of molecule  $i$  and site B of molecule  $j$ , and this term can be estimated using Eq. (3), where the parameters  $\varepsilon^{A_i, B_j}$  &  $\beta^{A_i, B_j}$  in Eq. (3) are the association energy and association volume between site A on molecule  $i$  and site B on molecule  $j$ , respectively, and the parameter  $g$  is an important parameter for CPA EoS known as the radial distribution function.

$$\Delta^{A_i, B_j} = g(\rho) \left[ \exp\left(\frac{\varepsilon^{A_i, B_j}}{RT}\right) - 1 \right] b_{ij} \beta^{A_i, B_j}, \quad b_{ij} = \frac{b_i + b_j}{2} \quad (3-3)$$

Parameters  $a(T)$  and  $g$  can be expressed by Eqs. (4) and (5), respectively.

$$a(T) = a_0 \left( 1 + m(1 - T_r^{0.5}) \right)^2 \quad (3-4)$$

where  $T_r (=T/T_c)$  and  $T_c$  are the reduced temperature and critical temperature, respectively, and  $m$  is correlated with the acentric factor.

$$g(\rho_m) = \frac{1}{1-1.9\eta}, \quad \eta = \frac{1}{4}b\rho_m \quad (3-5)$$

### **3-5-2 Non-Random Two Liquid (NRTL) model**

The Non-Random Two Liquid (NRTL) model proposed by Renon and Prausnitz in 1968 [30] is an activity coefficient-based model that correlates the activity coefficient ( $\gamma$ ) of molecules present in the liquid phase. In this model, the excess Gibbs energy is used to describe the nonideality of the liquid phase, where the gas phase is considered an ideal gas. NRTL model uses Eq. (6) to (8) to estimate the activity coefficient of component  $i$  ( $\gamma_i$ ) in the liquid mixture.

$$\ln(\gamma_i) = \frac{\sum_j \tau_{ji} G_{ji} x_j}{\sum_k G_{ki} x_k} + \sum_j \frac{x_j G_{ij}}{\sum_k G_{ki} x_k} \left[ \tau_{ij} - \frac{\sum_l \tau_{lj} G_{lj} x_l}{\sum_k G_{kj} x_k} \right] \quad (3-6)$$

$$G_{ij} = \exp(-\alpha_{ij} \tau_{ij}) \quad (3-7)$$

$$\tau_{ij} = a_{ij} + \frac{b_{ij}}{T} \quad (3-8)$$

where  $\tau$  and  $\alpha$  are the binary interaction energy parameter and non-random factor parameter, respectively, and  $\tau_{ij} \neq \tau_{ji}$  and  $a_{ij} = a_{ji}$ .

### **3-5-3 Models' parameters and data correlation**

For correlating the experimental vapor-liquid equilibrium (VLE) data ( $T, P, x, y$ ) of the binary mixture of n-C<sub>6</sub> and H<sub>2</sub>O with the CPA EoS model, one thermodynamic model based on the flash algorithm is developed with MATLAB software. CPA parameters, including physical and association parameters for the associating (water) and non-associating (n-hexane) components, are reported in Table 3-2 [27,31,32]. The binary interaction parameter ( $k_{ij}$ ) is calculated using the following equation [33], which is valid for water-alkane (from water-propane to water-decane):

$$k_{ij} = -0.026n + 0.1915 \quad (3-9)$$

Where  $n$  is the carbon number of the normal alkane.

Table 3-2: Parameters for CPA EoS for associating and non-associating components used in this study

Parameters	H <sub>2</sub> O	n-C <sub>6</sub>	Reference
$b$ (L/mol)	0.0145	0.1078	[27,31,32]
$a_0$ (bar.L <sup>2</sup> /mol <sup>2</sup> )	1.2277	23.9340	[27,31,32]
$c_1$	0.6736	0.83130	[27,31,32]
$\epsilon^{AB}$ (bar.L.mol <sup>-1</sup> )	166.55	-	[27,31,32]
$\beta^{AB}$	0.0692	-	[27]
$T_c$	647.29	522.32	[27]

Aspen Plus V12.1 was also used to correlate the vapor-liquid equilibrium (VLE) data using the NRTL model. Parameters  $\tau$  and  $\alpha$  were determined by the regression of the experimental data with the data regression system (DRS) incorporated in Aspen. The Britt-Luecke algorithm was used for regression to minimize the errors in all measured variables by using the maximum likelihood objective function (OF) shown in Eq. (10) [34].

$$OF = \sum_{i=1}^N \left[ \left( \frac{T_E - T_M}{\sigma_T} \right)^2 + \left( \frac{P_E - P_M}{\sigma_P} \right)^2 + \left( \frac{x_E^{C_6} - x_M^{C_6}}{\sigma_x} \right)^2 + \left( \frac{y_E^{C_6} - y_M^{C_6}}{\sigma_y} \right)^2 \right] \quad (3-10)$$

### **3-6 Results and Discussion**

The vapor-liquid equilibria (VLE) of the binary mixture of n-C<sub>6</sub>/H<sub>2</sub>O system at ~2.5 MPa and the temperature range of 183.7-214.7 °C were measured and reported in Table 3. In some experiments, the system pressure slightly deviated from the desired pressure of 2.5 MPa. The actual system pressure is reported in Table 3-3, along with the system temperature. VLE results of the present study are graphically presented as a  $T$ - $xy$  diagram in Figure 3-4. For each experiment, more than ten vapor phase samples were analyzed with gas chromatography (GC), and the average mole fraction and standard deviation were estimated. The range of standard deviation of the analyses varies from 0.0036 to 0.0159 (with an average standard deviation of

0.0090). For each experiment, at least two liquid phase samples were collected and analyzed with GC. The observed water concentration in the hydrocarbon-rich phase was insignificant. Experimental results show that the bubble point line for the phase diagram of the C<sub>6</sub>/H<sub>2</sub>O binary system is around 183.7 °C, including an azeotropic point close to 0.6029 mole-fraction of C<sub>6</sub>. When the concentration of C<sub>6</sub> in the binary mixture was below the azeotropic point concentration, the vapor phase was at equilibrium with mostly liquid water with a very low concentration of C<sub>6</sub> ( $\leq 0.0002$  mole-fraction of C<sub>6</sub>) for the studied temperature range and pressure. On the other hand, the vapor phase was at equilibrium with mostly liquid C<sub>6</sub> when the overall concentration of C<sub>6</sub> was above the azeotropic point. At 2.50 MPa, the mole-fraction of C<sub>6</sub> in the vapor phase varies from 0 to  $\sim 0.6029$  below the azeotropic concentration in the range of temperature from 223.95 °C (boiling point of H<sub>2</sub>O) to the azeotropic point ( $\sim 183.7$  °C). Above the azeotropic concentration of C<sub>6</sub>, the vapor phase concentration varies from  $\sim 0.6029$  to 1 for the temperature range of  $\sim 183.7$  °C to 221.33 °C (boiling point of C<sub>6</sub>). The area below the bubble point line in the  $T$ - $xy$  diagram is the liquid-liquid equilibria (LLE) region, where the hydrocarbon-rich liquid phase is in equilibrium with the water-rich phase at a temperature below the azeotropic point. The areas enclosed by the bubble point line and dew point line are also two-phase regions representing the vapor-liquid equilibria (VLE). The area over the dew point line is a single-phase region with only the vapor phase.

The model predicted VLE ( $T$ - $xy$ ) data previously reported in literature showed a similar trend with the co-condensation temperature of 173.1 °C at 0.575-molefraction of n-C<sub>6</sub> at 2.0 MPa [22] and 182 °C at 0.64 mole fraction of n-C<sub>6</sub> at 2.5 MPa [6].

Table 3-3: Experimental vapor-liquid equilibria (VLE) data ( $T$ ,  $P$ ,  $x$ ,  $y$ ) for the binary mixture of n-C<sub>6</sub>/H<sub>2</sub>O system.

Temperature, T (°C)	Pressure, P (MPa)	Mole fraction of C <sub>6</sub> in the vapor phase, $y_{C_6}$	Mole fraction of H <sub>2</sub> O in the vapor phase, $y_{H_2O}$	Mole fraction of C <sub>6</sub> in the liquid phase, $x_{C_6}$	Mole fraction of H <sub>2</sub> O in the liquid phase, $x_{H_2O}$
<b>Water Rich sample (Left side of the azeotrope)</b>					
183.7	2.48	0.6029	0.3971	0.0002	0.9998
186.6	2.50	0.5381	0.4619	0.0002	0.9998
190.5	2.50	0.4764	0.5236	0.0002	0.9998
195.3	2.50	0.4323	0.5677	0.0002	0.9998
195.3	2.50	0.4362	0.5638	0.0002	0.9998
200.2	2.50	0.3604	0.6396	0.0002	0.9998
205	2.50	0.2954	0.7046	0.0002	0.9998
209.9	2.50	0.2272	0.7728	0.0001	0.9999
214.7	2.50	0.1516	0.8484	0.0001	0.9999
<b>Hydrocarbon Rich sample (Right side of the azeotrope)</b>					
185.7	2.64	0.6254	0.3746	1.0000	0.0000
185.7	2.53	0.6342	0.3658	1.0000	0.0000
190.5	2.62	0.6804	0.3196	1.0000	0.0000
195.3	2.64	0.7498	0.2502	1.0000	0.0000
200.2	2.52	0.8054	0.1946	1.0000	0.0000
205.0	2.45	0.8694	0.1306	1.0000	0.0000
209.9	2.63	0.8738	0.1262	1.0000	0.0000

\* Standard uncertainties u are u(T) = 0.5 °C, u(P) = 0.003 MPa, and the relative expanded uncertainties (Ur) are: Ur(x) = 0.0001, Ur(y) = 0.0114.

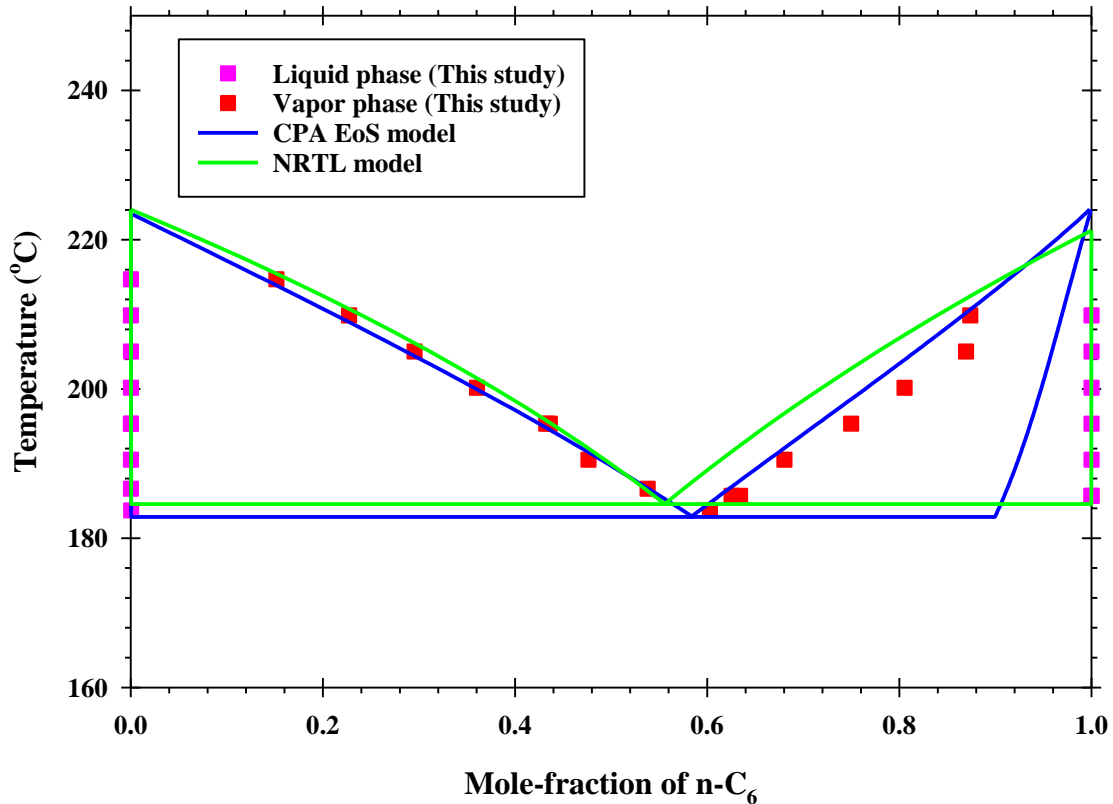


Figure 3-4: Vapor-liquid equilibria (T-xy) of n-C<sub>6</sub>/ H<sub>2</sub>O binary system at ~2.5 MPa.

Experimental data: ■, mole-fraction of n-C<sub>6</sub> in the liquid phase (bubble point), and ■, mole-fraction of n-C<sub>6</sub> in the vapor phase (dew point). The model predicted data: Solid line [blue and green lines represent predicted VLE data by CPA EoS model and NRTL model, respectively].

Experimental vapor-liquid equilibria (VLE) data ( $T$ ,  $P$ ,  $x$ ,  $y$ ) were modeled with the CPA EoS. The CPA model predicted mole-fraction of n-C<sub>6</sub> in vapor-phase and liquid-phase at the corresponding temperature and pressure. Results are compared with the experimental VLE data in Figure 3-4 and the plot shows that the CPA model reproduced the experimental data on the entire range of composition with acceptable accuracy. The overall root means square deviation (RMSD) of the n-C<sub>6</sub> mole-fraction in vapor and liquid phases for CPA EoS model is 0.0234.

The experimental VLE data were also modeled with the NRTL model, and predicted  $T$ - $xy$  data at 2.5 MPa for the n-C<sub>6</sub>/H<sub>2</sub>O system are compared with the experimental data in Figure 3-4. Regressed NRTL parameters for n-C<sub>6</sub>/H<sub>2</sub>O system is reported in Table 3-4. The non-randomness factors  $\alpha_{ij}$  were pre-fixed at 0.2 during the regression. The RMSD between the predicted n-C<sub>6</sub> mole-fraction and experimental results in vapor-phase and liquid phase were 0.0765 and  $1.6029 \times 10^{-6}$ . The overall RMSD of the n-C<sub>6</sub> mole-fraction in vapor and liquid phases for NRTL model is 0.0765, respectively.

The developed NRTL thermodynamic model is also used to predict the liquid-liquid equilibria ( $T$ - $xx$ ) of the n-C<sub>6</sub>/H<sub>2</sub>O binary system at 0.1 MPa ( $\pm 0.01$ ) and compared with the literature [10–15] in Figure 3-5. The predicted  $T$ - $xx$  data were found to be in good agreement with the previously published literature. Note the reported hexane and water experimental mole fraction ranges of (b)  $x_{n\text{-C}_6}^{\text{water}} < 1 \times 10^{-3}$  (water-rich phase), (c)  $1 \times 10^{-6} < x_{\text{H}_2\text{O}}^{\text{Oleic}} < 0.1$  (hexane-rich phase), respectively.

Table 3-4: Regressed NRTL parameters for n-C<sub>6</sub>/H<sub>2</sub>O system.

Components	$a_{12}$	$a_{21}$	$b_{12}$	$b_{21}$	$\alpha$
n-C <sub>6</sub> (1)-H <sub>2</sub> O(2)	0	0	3166.49	3006.17	0.2

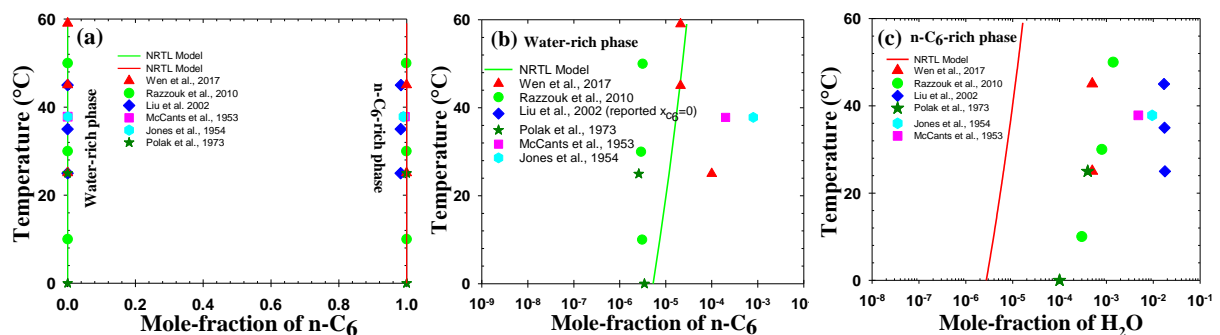


Figure 3-5: Comparison of the predicted liquid-liquid equilibria ( $T$ - $xx$ ) for n-C<sub>6</sub>/H<sub>2</sub>O binary system using NRTL model with the previously published data in literature at 0.1 MPa ( $\pm 0.01$ ) [10–15].

(solid line: model prediction, and symbol: experiment) (a) Temperature versus mole-fraction of n-C<sub>6</sub> (T-xx) in water-rich phase and n-C<sub>6</sub> rich phase (b) Temperature versus mole-fraction of n-C<sub>6</sub> in water-rich phase (semi log scale), (c) Temperature versus mole-fraction of H<sub>2</sub>O in n-C<sub>6</sub>-rich phase (semi log scale). Note the reported hexane and water experimental mole fraction ranges of (b)  $x_{nC_6}^{water} < 1 \times 10^{-3}$  (water-rich phase), (c)  $1 \times 10^{-6} < x_{H_2O}^{Oleic} < 0.1$  (hexane- rich phase), respectively.

The activity coefficient ( $\gamma$ ) demonstrates the non-ideality of a component in a mixture. Deviation from the ideality of the component in a mixture can be estimated from the activity coefficient [35,36]; where the infinite dilution activity coefficients ( $\gamma^\infty$ ) demonstrates the greatest degree of non-ideality of the mixture [35,36]. The infinite dilution activity coefficient is of great interest due to its usefulness in the estimation of vapor-liquid equilibria [35,36]. The activity coefficient of the n-C<sub>6</sub> and H<sub>2</sub>O at the temperature range from 185 to 220 °C and 2.5 MPa were estimated using the NRTL model and reported in Table 3-5. The estimated activity coefficient of H<sub>2</sub>O ( $\gamma_{H_2O}$ ) in water-rich phase and the activity coefficient of n-C<sub>6</sub> ( $\gamma_{C_6}$ ) in n-C<sub>6</sub> rich phase was one (1).  $\gamma^\infty$  of n-C<sub>6</sub> and H<sub>2</sub>O were also estimated using  $\ln \gamma_2^\infty = \tau_{12} (1 + \exp(-\alpha_{12} \tau_{21}))$  [37], and reported in Table 3-5.

Table 3-5: The activity coefficient of the n-C<sub>6</sub> and H<sub>2</sub>O.

Temperature (°C)	H <sub>2</sub> O rich phase		n-C <sub>6</sub> rich phase		$\ln \gamma_{C_6}^\infty$	$\ln \gamma_{H_2O}^\infty$
	$\ln \gamma_{C_6}$	$\ln \gamma_{H_2O}$	$\ln \gamma_{H_2O}$	$\ln \gamma_{C_6}$		
185	8.284	0	8.668	0	8.296	8.678
190	8.222	0	8.601	0	8.233	8.609
195	8.161	0	8.535	0	8.170	8.542
200	8.101	0	8.470	0	8.109	8.475
205	8.042	0	8.407	0	8.048	8.410
210	7.985	0	8.344	0	7.989	8.346
215	7.928	0	8.282	0	7.931	8.284
220	7.872	0	8.222	0	7.874	8.222

### **3-7 Conclusion**

Vapor-liquid equilibria (VLE) of hydrocarbon solvents and steam binary mixture are important for the feasibility studies of the solvent-aided thermal recovery of bitumen. In this work, VLE studies were carried out at ~2.5 MPa and a temperature range from 183.7-214.7 °C. The temperature-composition data indicates that the system exhibits an azeotrope at ~0.6029 n-C<sub>6</sub> mole fraction when the temperature is ~183.7 °C. This study revealed that the condensed liquid phase primarily contains water below the solvent azeotropic concentration. On the other hand, above the solvent azeotropic concentration, the condensed liquid is mainly water. The experimental data were modeled using the CPA-EoS and NRTL model. Activity coefficient ( $\gamma$ ) and infinite dilution activity coefficient ( $\gamma^\infty$ ) of n-C<sub>6</sub> and H<sub>2</sub>O were estimated and reported in this study. The root means square deviation (RMSD) of the n-C<sub>6</sub> mole-fraction in vapor and liquid phases for CPA EoS and NRTL model are 0.0234 and 5.86%, respectively.

### **3-8 References**

- [1] N. Haarmann, S. Enders, G. Sadowski, Modeling binary mixtures of n-alkanes and water using PC-SAFT, *Fluid Phase Equilib.* 470 (2018) 203–211. <https://doi.org/https://doi.org/10.1016/j.fluid.2017.11.015>.
- [2] J.-H. Kim, Y.-K. Ryu, S. Haam, C.-H. Lee, W.-S. Kim, adsorption and steam regeneration of n-hexane, mek, and toluene on activated carbon fiber, *Sep Sci Technol.* 36 (2001) 263–281. <https://doi.org/10.1081/SS-100001078>.
- [3] F.M. Bkangmo Kontchouo, Z. Gao, X. Xianglin, Y. Wang, Y. Sun, S. Zhang, X. Hu, Steam reforming of n-hexane and toluene: Understanding impacts of structural difference of aliphatic and aromatic hydrocarbons on their coking behaviors, *J Environ Chem Eng.* 9 (2021) 106383. <https://doi.org/https://doi.org/10.1016/j.jece.2021.106383>.
- [4] P.A. Govind, S. Das, S. Srinivasan, T. Wheeler, Expanding Solvent SAGD in Heavy Oil Reservoirs, in: SPE, ConocoPhillips Company 2008 SPE International Thermal Operations and Heavy Oil Symposium, SPE, Canada, 2008. <https://doi.org/10.2118/117571-MS>.
- [5] N. Sabet, H. Hassanzadeh, J. Abedi, Selection of efficient solvent in solvent-aided thermal recovery of bitumen, *Chem Eng Sci.* 161 (2017) 198–205. <https://doi.org/https://doi.org/10.1016/j.ces.2016.12.031>.
- [6] R. Khaledi, T.J. Boone, H.R. Motahhari, G. Subramanian, Optimized Solvent for Solvent Assisted-Steam Assisted Gravity Drainage (SA-SAGD) Recovery Process, in: Paper Presented at the SPE Canada Heavy Oil Technical Conference, SPE, Calgary, Alberta, Canada, 2015. <https://doi.org/10.2118/174429-MS>.
- [7] H. Nourozieh, M. Kariznovi, J. Abedi, SPE-170163-MS Phase Behavior Study of Butane / Athabasca Bitumen Mixtures Applicable for Thermal and Hybrid Solvent Recovery Processes, 2014. <http://onepetro.org/SPECHOC/proceedingspdf/14HOCC/314HOCC/D031S014R007/1547294/spe-170163-ms.pdf/1>.

- [8] M. Al-Murayri, B. Maini, T. Harding, J. Oskouei, Multicomponent Solvent Co-injection with Steam in Heavy and Extra-Heavy Oil Reservoirs, *Energy & Fuels*. 30 (2016). <https://doi.org/10.1021/acs.energyfuels.5b02774>.
- [9] H. Sadeghi Yamchi, M. Zirrahi, H. Hassanzadeh, J. Abedi, Measurements and NRTL modeling of liquid-liquid equilibrium of dimethyl ether/bitumen, *Fluid Phase Equilib.* 512 (2020) 112549. <https://doi.org/10.1016/j.fluid.2020.112549>.
- [10] J. Liu, Z. Qin, J. Wang, Liquid–Liquid Equilibria for Methanol + Water + Hexane Ternary Mixtures, *J Chem Eng Data*. 47 (2002) 1243–1245. <https://doi.org/10.1021/je0255269>.
- [11] A. Razzouk, R.A. Naccoul, I. Mokbel, P. Duchet-Suchaux, J. Jose, E. Rauzy, C. Berro, Liquid–Liquid Equilibria for Monoethylene Glycol + Hexane and 2,2,4-Trimethylpentane, Water + Hexane and 2,2,4-Trimethylpentane, Monoethylene Glycol + Water + Hexane, and Monoethylene Glycol + Water + 2,2,4-Trimethylpentane in the Temperature Range between  $T = 283.15$  K and  $T = 323.15$  K, *J Chem Eng Data*. 55 (2010) 1468–1472. <https://doi.org/10.1021/je900295u>.
- [12] L. Wen, N. Zhang, H. Li, Q. Huang, X. Wu, X. Hao, M. Wu, C. Ban, J. Zhao, Ternary Liquid–Liquid Equilibrium for Mixtures of Water + ( $\pm$ ) $\alpha$ -Phenylethylamine + n-Hexane at  $T = 298.2$ ,  $318.2$ , and  $333.2$  K, *J Chem Eng Data*. 62 (2017) 1819–1824. <https://doi.org/10.1021/acs.jced.6b01064>.
- [13] J.F. McCants, J.H. Jones, W.H. Hopson, Ternary Solubility Data for Systems Involving 1-Propanol and Water, *Ind Eng Chem*. 45 (1953) 454–456. <https://doi.org/10.1021/ie50518a054>.
- [14] J.H. Jones, J.F. McCants, Ternary Solubility Data, *Ind Eng Chem*. 46 (1954) 1956–1958. <https://doi.org/10.1021/ie50537a052>.
- [15] J. Polak, B.C.-Y. Lu, Mutual Solubilities of Hydrocarbons and Water at 0 and 25 °C, *Can J Chem*. 51 (1973) 4018–4023. <https://doi.org/10.1139/v73-599>.

- [16] C. Tsonopoulos, G.M. Wilson, High-temperature mutual solubilities of hydrocarbons and water. Part I: Benzene, cyclohexane and n-hexane, *Aiche Journal*. 29 (1983) 990–999.
- [17] Th.W De Loos, W.G Penders, R.N Lichtenthaler, Phase equilibria and critical phenomena in fluid (n-hexane + water) at high pressures and temperatures, *The Journal of Chemical Thermodynamics* Volume 14, Issue 1,. 14 (1982) 83–91.
- [18] E. Brunner, Fluid mixtures at high pressures IX. Phase separation and critical phenomena in 23 (n-alkane + water) mixtures, *J Chem Thermodyn*. 22 (1990) 335–353.
- [19] S. M. Rasulov, I. A. Isaev, S. M. Orakova, Phase Equilibrium and Critical Phenomena in the n-Pentan–Water and n-Hexane–Water Systems at High Temperatures and Pressures, *Russian Physics Journal*. 61 (2018) 781–789.
- [20] I.M. Abdulagatov, A.R. Bazaev, E.A. Bazaev, B.K. Osmanova, Experimental study of PVT and phase-transition properties of binary water+n-hexane mixture near the upper critical endpoint, *J Mol Liq*. 323 (2021).
- [21] M. Burrufet, K. Liu, S. Rahmann, C. Wu, Simultaneous Vapor-Liquid-Liquid Equilibria and Phase Molar Densities of a Quaternary System of Propane + Pentane + Octane + Water, *J Chem Eng Data*. 41 (1996) 918–922.
- [22] L. Dong, Effect of vapour–liquid phase behavior of steam–light hydrocarbon systems on steam assisted gravity drainage process for bitumen recovery, *Fuel*. 95 (2012) 159–168.
- [23] J. Shim, J.P. Kohn, Multiphase and Volumetric Equilibria of Methane-n-Hexane Binary System at Temperatures between —110° and 150° C, *J Chem Eng Data*. 7 (1962).
- [24] M.J. Cebola, W.A. Wakeham, G. Saville, V.l.e. measurements at high pressures and high temperatures on (methane + n-hexane), *Journal of Chemical Thermodynamics*. 32 (2000) 1265–1284.

- [25] K. Chylinski, M.J. Cebola, A. Meredith, G. Saville, W.A. Wakeham, Apparatus for phase equilibrium measurements at high temperatures and pressures, *Journal of Chemical Thermodynamics*. 34 (2002) 1703–1728.
- [26] P. Marteau, J. Obriot, A. Barreau, V. Ruffier-Meray, E. Behar, Experimental determination of the phase behavior of binary mixtures: methane-hexane and methane-benzene, *Fluid Phase Equilib.* 129 (1997) 285–305.
- [27] G. M. Kontogeorgis, M. L. Michelsen, G. K. Folas, S. Derawi, N. V. Solms, E. H. Stenby, Ten Years with the CPA (Cubic-Plus-Association) Equation of State. Part 1. Pure Compounds and Self-Associating Systems, *Ind Eng Chem Res.* 45 (2006) 4855–4868.
- [28] G. M. Kontogeorgis, E. C. Voutsas, I. V. Yakoumis, D. P. Tassios, An Equation of State for Associating Fluids, *Ind Eng Chem Res.* 35 (1996) 4310–4218.
- [29] G. Soave, Equilibrium constants from a modified Redlich-Kwong equation of state, *Chem Eng Sci.* 27 (1972) 1197–1203.
- [30] H. Renon, J. M. Prausnitz, Local Compositions in Thermodynamic Excess Functions for Liquid Mixtures, *American Institute of Chemical Engineers.* 14 (1968) 135–144.
- [31] M.B. Oliveira, J.A.P. Coutinho, A.J. Queimada, Mutual solubilities of hydrocarbons and water with the CPA EoS, *Fluid Phase Equilib.* 258 (2007) 58–66.
- [32] G. K. Folas, G. M. Kontogeorgis, M. L. Michelsen, E. H. Stenby, Application of the Cubic-Plus-Association (CPA) Equation of State to Complex Mixtures with Aromatic Hydrocarbons, *Ind Eng Chem Res.* 45 (2006) 1527–1538.
- [33] G. M. Kontogeorgis, Georgios K Folas, *Thermodynamic models for industrial applications: from classical and advanced mixing rules to association theories*, Wiley and Sons. , 2009.
- [34] J. Li, C. Hua, S. Xiong, F. Bai, P. Lu, J. Ye, Vapor-Liquid Equilibrium for Binary Systems of Allyl Alcohol + Water and Allyl Alcohol + Benzene at 101.3 kPa., *J Chem Eng Data.* 62 (2017) 3004–3008.

- [35] E. C. Voutsas, D. P. Tassios, Prediction of Infinite-Dilution Activity Coefficients in Binary Mixtures with UNIFAC. A Critical Evaluation, *Ind Eng Chem Res.* 35 (1996) 1438–1445.
- [36] S. Zhang, T. Hiaki, M. Hongo, K. Kojima, Prediction of infinite dilution activity coefficients in aqueous solutions by group contribution models. A critical evaluation, *Fluid Phase Equilib.* 144 (1998) 97–112.
- [37] M.D. Hilliard, A predictive thermodynamic model for an aqueous blend of potassium carbonate, piperazine, and monoethanolamine for carbon dioxide capture from flue gas, The university of Texas at Austin, 2008.

## **Chapter 4: Vapor-liquid-liquid equilibrium (VLLE) of the ternary mixtures of normal hexane, water and bitumen at T=185-210 °C and at P= 2.5 MPa**

### **4-1 Abstract**

In this chapter, vapor-liquid-liquid equilibrium (VLLE) of the ternary system of normal-hexane, water and Mackay River bitumen mixture is studied at temperatures ranging from 185-210 °C and at a pressure of 2.5 MPa. The concentration of solvent/steam (n-C<sub>6</sub>/H<sub>2</sub>O) was varied to understand the effect of solvent (n-C<sub>6</sub>) on the phase behavior and the thermophysical properties of the associated phases. Two solvent mole fractions of 0.01 and 0.05 (6.85 and 27.7 vol.%) of water/hexane were considered. The mole fraction of hexane in a mixture of bitumen/solvent was maintained at 0.7 (37.45 vol.%), near the maximum solubility of hexane in bitumen/solvent at the operational condition of solvent-aided thermal recovery processes of bitumen from oil sands. In addition to the VLLE phase equilibria study, the viscosity and density of the two distinct liquid phases, hydrocarbon-rich oleic and water-rich aqueous phases, were measured and reported. The results infer that the concentration of n-C<sub>6</sub> coinjected with steam does not significantly affect the equilibrium phase concentrations of phases and thermophysical properties. Furthermore, the results suggest that the presence of bitumen in equilibrium does not significantly affect the solvent content of the vapor phase compared with the vapor phase of the n-C<sub>6</sub>/H<sub>2</sub>O binary mixture. The findings provide insight into steam/solvent condensation behavior with applications to the solvent-aided thermal recovery of bitumen from oil sands.

### **4-2 Introduction**

Steam-assisted gravity drainage (SAGD) has been the primary thermal recovery method for in-situ bitumen recovery from oil sands reservoirs. The SAGD process requires high energy for steam generation, resulting in high greenhouse gas emissions. Due to the high energy requirement of the SAGD process, solvent-assisted SAGD (SA-SAGD) processes and

heated solvent processes have gained great emphasis. In the SA-SAGD process, the idea of solvent co-injection has shown promise in terms of speeding bitumen recovery and reducing the operation's energy intensity. According to experimental work done by the Alberta Research Council (ARC) and Imperial [1], adding solvent to steam caused bitumen recovery rates to increase. At the same time, steam-oil ratios (SOR) fall compared to the standard SAGD process. Imperial Oil Resources performed solvent-assisted SAGD (SA-SAGD) pilot testing on Cold Lake bitumen at 3.6 MPa operating pressure [2]. The result of the field testing showed a positive impact on bitumen production and SOR reduction. Gupta and Gittins [3] reported a 150 tonne/day increase in bitumen production from the use of butane in the solvent-assisted pilot test on EnCana's Christina Lake project. Also, the use of butane as a solvent for the pilot test resulted in upgraded oil production. The positive outcomes of the pilot testing triggered more research work on the topic. It has been recommended that for an effective viscosity reduction, the coinjected solvent-steam is maintained in the vapor phase until it reaches the bitumen interface, where co-condensation takes place [4]. Injected solvent dilutes in the bitumen to reduce the viscosity. At the same time, steam transfers its latent heat into bitumen and mobilizes the bitumen to the producer well with the help of gravity [5]. A significant challenge is the complex thermodynamic phase behavior of solvent-water-bitumen systems, which requires a better understanding. Depending on the SA-SAGD operating condition, a liquid-liquid (L-L), vapor-liquid (V-L), or vapor-liquid-liquid equilibrium phase may develop [6]. Depending on the equilibrium condition, the solubility of the solvent in the bitumen may vary. Hence, the thermophysical properties of the oleic phase are affected. In addition, the co-injection of multicomponent solvent (condensate) and steam for bitumen recovery investigated using a large-scale physical model resulted in asphaltene production [7]. As a result, the phase behavior, viscosity, and density measurements of solvent-steam-bitumen systems play a crucial role in the feasibility and design of SA-SAGD processes.

Various hydrocarbon solvents have been considered for SA-SAGD methods since solvent-aided processes have gained popularity. One common assumption is that SA-SAGD performs better with solvents with saturation temperatures comparable to steam [1]. Different hydrocarbon solvents, including light to medium n-alkane (C<sub>1</sub>-C<sub>6</sub>), carbon dioxide (CO<sub>2</sub>), and ammonia, have been investigated and/or their thermophysical properties, mostly in the absence of water, have been measured [8,9]. Fu et al. [10] studied the solubility of C<sub>1</sub> and C<sub>2</sub> on Cold Lake bitumen at a temperature range from 65-150 °C and up to 12 MPa. The solubility, viscosity, and density of the propane-saturated Athabasca bitumen were measured experimentally by Nourzieh et al., [11] at 50-200 °C and up to 10 MPa. They study used PR-EoS to correlate the solvent-saturated bitumen solubility and density, while Pedersen's method was implemented for viscosity correlation. Dini et al., [12] performed a detailed study of the solubility of C<sub>3</sub> in Peace River bitumen using X-ray view cell apparatus at operating conditions below the critical temperature and pressure of propane. Solubilities of hydrocarbon solvent from C<sub>1</sub>-C<sub>4</sub> were investigated by Zirrahi et al., [13] at temperatures 100, 150, and 190 °C and up to 4.5 MPa in the presence and absence of water. At any given temperature and pressure, heavier solvents were more soluble in bitumen, and the solubility values decreased as temperature increased. The ternary systems were compared to solvent/bitumen systems under the same condition to study the effect of water on the mixture viscosity and density. It was shown that the addition of water increased viscosity reduction, but this effect was dominant at lower temperatures. Additionally, the authors correlated the solubility of the solvent-saturated bitumen using PR-EoS and used a mixing rule to correlate the mixture viscosity. Haddadnia et al., [14] extended Zirrahi et al.,[13] work by measuring the solubility and thermophysical properties of C<sub>1</sub>-C<sub>4</sub> saturated bitumen at elevated temperature and pressure up to 260 °C and 6 MPa, respectively. The solubilities of heavier solvents were found to decrease significantly at high temperatures. The density and viscosity of mixtures of bitumen/C<sub>5</sub> and bitumen/C<sub>6</sub>

mixtures were also measured by Haddadnia et al. [15]. Yamchi et al., [16] studied the LLE of various mixtures and measured the viscosity and density of C<sub>4</sub>/bitumen system and C<sub>4</sub>/additive/bitumen system at a pressure above the solvent vapor pressure and temperatures of 40 and 60 °C. Propane, toluene and Dimethyl Ether (DME) were used as additives in their study. The effect of C<sub>3</sub> was studied for 10 wt.% and 20 w.t% concentrations at 2.8 MPa to ensure LLE conditions. A lower light liquid phase density was observed with an increase in the C<sub>3</sub> weight concentration due to asphaltene precipitation.

In addition to hydrocarbon solvents, bio-based solvents have also received significant attention due to minimized environmental impacts compared to hydrocarbon solvents. Haddadnia et al., [17] reported thermophysical properties of DME/Athabasca bitumen at temperatures 100, 125, and 150 °C and up to 6 MPa. The thermophysical properties of DME/Athabasca bitumen were compared with those of butane/bitumen and propane/bitumen systems. They reported that all measured parameters for the DME/bitumen system fall between propane and butane systems. Hence it was concluded that DME could effectively substitute butane and propane solvents in SA-SAGD processes. Additionally, the experimental solubility data were predicted with PR-EoS, and the viscosity of the solvent-saturated bitumen was correlated using the Pederson corresponding state model. Yamchi et al., [18] also measured and modeled the LLE of DME/bitumen at different concentrations ranging from 60-80 wt.% and temperatures from 40-100 °C. Density and viscosity measurements from the studies showed a decreasing trend with DME weight percent. The NRTL model was used to model the LLE of DME/bitumen system. BinDahbag et al., [19] studied the VLE of ammonia/Athabasca bitumen at temperatures up to 190 °C and pressure from 1-4 MPa. Ammonia solubility in bitumen decreased with an increase in temperature at a constant pressure. A similar trend was observed for the viscosity and density of the ammonia/Athabasca bitumen mixtures.

Aside from time-consuming and expensive experimental measurements, predictive models are developed to measure solvent solubilities in various bitumen. Abdi et al., [17] modeled the VLLE of the bitumen-water-solvent ( $C_1$ ,  $C_2$ ,  $C_3$ ,  $C_4$ ,  $CO_2$ , and  $N_2$ ) mixture using the Cubic Plus Association (CPA) EoS model. The model assumed that there is no bitumen in the vapor and water-rich phase at any condition. Also, the bitumen was divided into pseudo-components, a saturated-rich compound (PC1) and an asphaltene-rich compound (PC2). Azinfar et al., [20] used a thermodynamic model to predict propane solubility in bitumen based on experimental fractionation and characterization. Athabasca and Cold Lake bitumen were fractionated into different cuts, with the cuts assumed to be the mixtures of n-alkanes. The developed model predicted propane-saturated bitumen solubilities, viscosity, and density with good agreement when compared to the experimental data. Water solubility in bitumen was studied and modelled by Zirrahi et al. [21] at thermal recovery operating conditions. The water solubility was modelled using PR-EoS with an average relative deviation (AARD) 8.4%.

Phase equilibria of the solvent-water-bitumen system and the associated thermophysical properties are necessary for the design and optimization of the solvent-assisted SAGD process. In addition, the solubility, viscosity, and density of such a system are essential for the phase behavior modeling that is required for thermal reservoir simulators. Furthermore, a detailed experimental observation of the steam/solvent co-condensation in the presence and absence of bitumen is lacking.

In this chapter, vapor-liquid-liquid equilibria of hexane ( $n-C_6$ )/water ( $H_2O$ )/Mackay River bitumen system is studied at a temperature range from 190-215 °C and pressure of 2.5 MPa. A test pressure of 2.5 MPa is used as the typical pressure of SA-SAGD operations. In addition to the phase equilibria, the viscosity and density of the liquid phases (hydrocarbon-rich and water-rich phases) are measured. The concentration of  $n-C_6/H_2O$  is varied to understand the effect of solvent on the phase behavior and the thermophysical properties.

Moreover, the measured data are modelled using the cubic-plus-association equation of state (CPA EoS).

The remaining of this chapter is structured as follows. First, the experimental materials, apparatus, and procedures are described. Then, the modeling approach using CPA EoS is presented, followed by results and conclusions.

## **4-3 Experimental**

### **4-3-1 Material**

The n-hexane was purchased from VWR with a minimum purity of 97 mol%. The sand-free Mackay River bitumen (MW = 523 g/mol) was provided by an oil sands company in Alberta. Details characterization of MacKay River bitumen was reported in the previous publications [22,23]. Di-ionized water used for the studies was prepared in the lab by boiling and degassing in a Sonicator. All chemicals used for the purpose of this study are listed in Table 4-1.

Table 4-1: Specifications of materials.

<b>IUPAC systematic name</b>	<b>CAS Registry Number</b>	<b>MW (g/mol)</b>	<b>Supplier</b>	<b>Purity<sup>a,b</sup> (%)</b>
Helium	CAS 7440-59-7	4.002	Linde Canada	99.999 mol%
Ethane	CAS 74-84-0	30.070	Linde Canada	99.00 wt%
n-hexane	CAS 110-54-3	86.180	VWR	97.00 wt%
n-Pentane	CAS 109-66-0	72.150	VWR	99.00 wt%
DI Water	CAS 7732-18-5	18.015	Prepared in Lab	-
Bitumen <sup>c</sup>	-	523.00	Provided by SHARP consortium	-

<sup>a</sup> Purity data was provided by the supplier.

<sup>b</sup> The provided chemicals were used directly in the experiments without further purification.

<sup>c</sup> Details characterization of MacKay River bitumen was reported in the previous publication [20,21].

### **4-3-2 Experimental Setup**

The experiment setup that was used in this study was developed and validated in our previous publication (Chukwuemeka et al.[24]).-The experimental setup shown in Figure 4-1 was used to study the vapor-liquid-liquid phase equilibria of n-C<sub>6</sub>-H<sub>2</sub>O-bitumen system. The experimental setup mainly consisted of a Blue-M oven, one rocking equilibrium cell (2,200 ml), a visual cell, a Quizix pump, a viscometer, and Gas Chromatography (GC). The

equilibrium cell, visual cell, and viscometer were placed inside the Blue-M oven, and the system temperature was controlled by the oven. However, the actual system temperature was measured using an external RTD probe to ensure accurate temperature measurements. The cell has a metal ball inside and an adjustable piston. The upward/downward movement of the piston regulates the cell volume and maintains the system at the equilibrium pressure. The metal ball moves as the cell rocks, agitating the sample and allowing for faster equilibrations. The Quizix pump maintains constant cell pressure by injecting or receiving the hydraulic fluid at 0.002 ml accuracy. A back pressure regulator (BPR) is installed after the visual cell to maintain the system pressure. A Hydramotion PVT viscometer (Hypervisc, model: HV1-702-C276-T350P700, maximum allowable working pressure: 206.8 MPa, maximum allowable working temperature: 350 °C) was placed after the equilibrium cell to measure dynamic fluid viscosity with an accuracy of 0.1 cP. The density of the liquid phases was determined using a pycnometer because of the high working temperatures; however, the density measurements using the pycnometer were highly prone to errors. Two separate Gas chromatography (Agilent Technologies GC 8890 and Shimadzu GC-2010) were used for the compositional analysis of the gas and liquid phase samples, respectively.

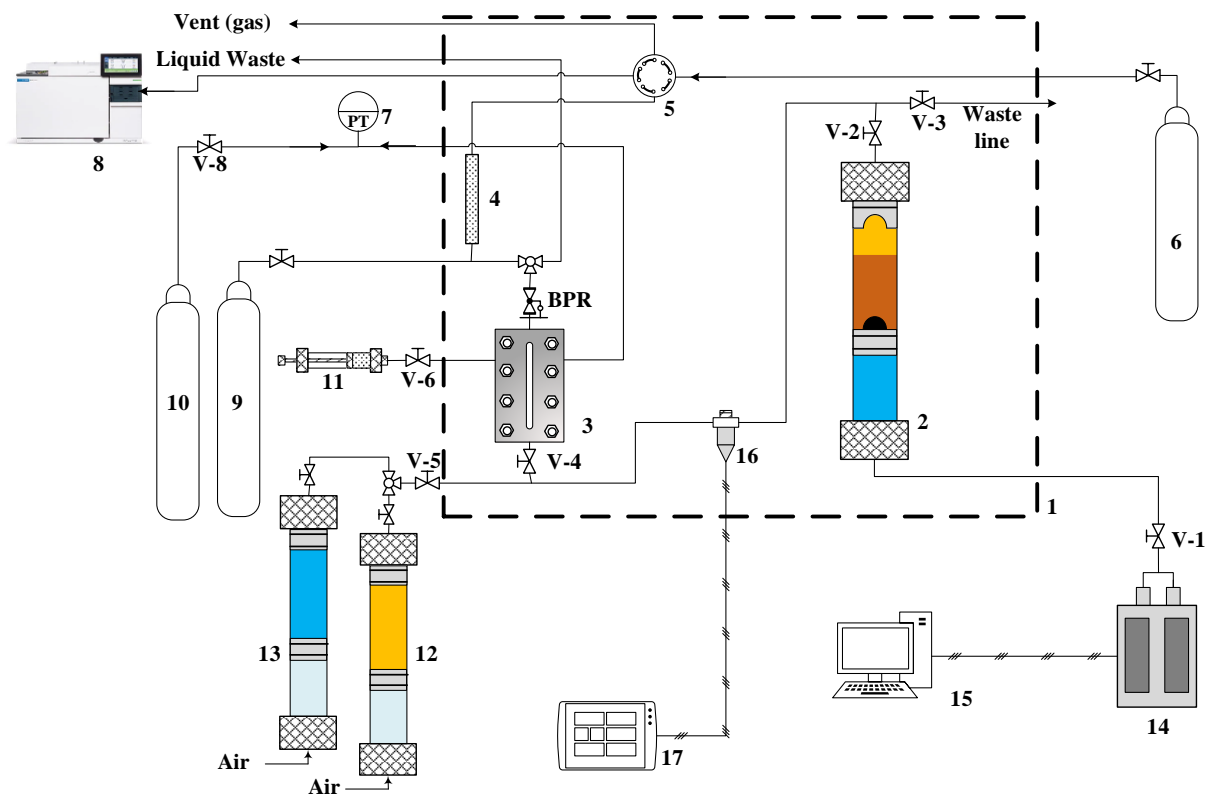


Figure 4-1: Experimental setup for n-hexane-water-bitumen VLLE studies. (1) Blue M oven, (2) Equilibrium cell, (3) Visual Cell, (4) Packed bed, (5) Ten-port valves, (6) Helium cylinder (Carrier Gas), (7) Pressure gauge, (8) Gas Chromatography (GC), (9) Gas Mixture cylinder (Ethane/Helium), (10) Helium cylinder, (11) liquid sample collector cell, (12) Distilled water feed cell, (13) n-Hexane feed cell, (14) Quizix pump, (15) Computer, (16) Viscometer, (17) Viscosity processor.

#### **4-3-3 Procedure**

Before each experiment, the entire system, including the equilibrium cell, the viscometer, and the flow lines were thoroughly cleaned with toluene, dried with acetone, and then vacuumed to remove any trapped air. The required amount of bitumen was charged into the equilibrium PVT cell followed by the H<sub>2</sub>O and n-C<sub>6</sub> depending on the (n-C<sub>6</sub> to H<sub>2</sub>O) and (n-C<sub>6</sub> to bitumen) concentration, and then the valve (V-2) placed at the top the PVT cell was closed. The Blue-M oven was set to the desired temperature, the pressure was set at 2.5 MPa,

and the equilibrium cell was set to rock until (more than 48 hours) the system reached equilibrium. Equilibrium was defined when the constant system volume was achieved. When equilibrium was attained, the cell was placed in the vertical position for a minimum of six hours to allow the phases to separate due to the differences in density. Hence the rest of the system was pressurized with helium, and the system pressure was controlled with the BPR at 2.5 MPa. Then, valve V-2 was opened, and the equilibrium phases were charged out of the cell using the Quizix pump by transferring the hydraulic fluid underneath the piston at a very low flow rate (~ 3 ml/min). Therefore, the piston moved upward and displaced the equilibrium samples placed at the top of the piston through the V-2 valve at a constant pressure. Displaced equilibrium samples were sequentially passed through the viscometer, visual cell, and BPR. Viscosity readings of the phases were taken while the phases were transferring through the viscometer. The phase boundaries of the equilibrium phases were indicated by a change in the viscosity reading on the viscometer. The visual cell placed before the BPR was used to monitor the gas and liquid phase samples. The gas phase accumulated on top of the liquid phases was passed through the BPR first, followed by the liquid-phase samples. The escaped gas phase sample from the BPR was transferred towards the Vent (gas) through a Ten-port valve (5). The concentration of the gas phase sample was analyzed by Gas Chromatography (GC) by transferring a particular volume of the sample to the TCD and FID GC systems using the Ten-port valve at frequent intervals. While the gas phase samples were sent directly to the GC system (Agilent Technologies GC 8890) for compositional analysis, at least two samples of each liquid phase (hydrocarbon-rich and water-rich) were collected utilizing a pressure-tight sample cell for compositional analysis using a GC system (Shimadzu GC-2010). The densities of the liquid phase samples were obtained using a pycnometer by collecting a known volume of liquid phase sample after the BPR through the liquid waste line and the weight of the bitumen was measured using a digital analytical balance (Secura® Precision Balance 3,100 gm,

sartorius lab instruments GmbH & Co. KG) with an accuracy of 10 mg. However, the density measurements using the pycnometer were highly prone to errors.

Figure 4-2 shows a separate experimental setup used to analyze both liquid-phase samples (hydrocarbon-rich and water-rich). The details of this experimental setup were reported in our previous publication [20]. Since it is not practical to vaporize bitumen due to very high boiling temperatures, a known amount of pentane ( $n\text{-C}_5$ ) was charged into the equilibrium cell (2) placed inside the oven with a known amount of hydrocarbon-rich sample. Hence, a small amount of high-pressure ethane was also charged from the ethane cell (5) to push the entire liquid sample inside the Equilibrium cell (2). The temperature of the equilibrium cell was maintained at  $180\text{ }^\circ\text{C}$  in an Oven. Sufficient time was provided for the complete evaporation of the  $n\text{-C}_5$ , water, and solvent ( $n\text{-C}_6$ ) contained inside the hydrocarbon-rich sample. The homogeneous mixture of  $\text{C}_2/n\text{-C}_5/n\text{-C}_6/\text{H}_2\text{O}$  was transferred to the gas sample outlet through a Ten-port valve. The composition of the homogeneous gas mixture then was analyzed by transferring a particular sample volume to the GC system (Shimadzu GC-2010). The amount of water and  $n\text{-C}_6$  contained inside the known amount of hydrocarbon-rich sample was estimated from the known amount of  $n\text{-C}_5$ .

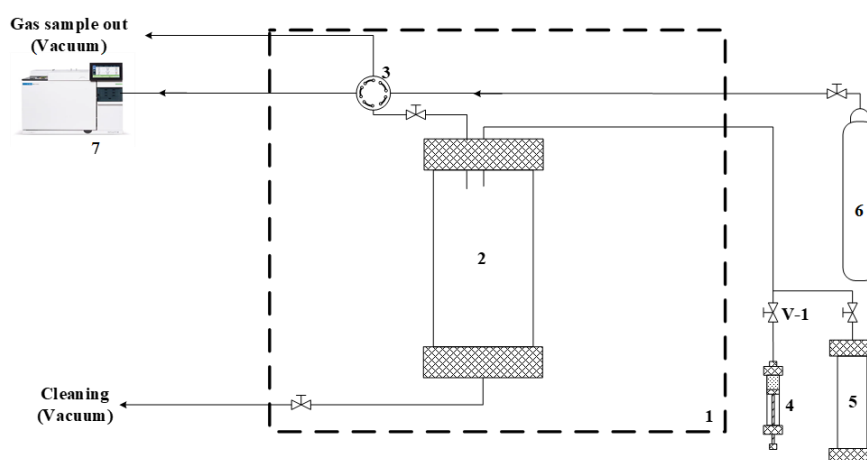


Figure 4-2: Liquid phase GC setup. (1) Blue M oven, (2) Equilibrium cell, (3) Ten-port valve, (4) Collector cell, (5) Ethane, (6) Helium, and (7) GC.

#### **4-4 Thermodynamic Modeling**

The experimental vapor-liquid-liquid equilibrium data of n-C<sub>6</sub>/H<sub>2</sub>O/bitumen system were modeled in this study. A Cubic Plus Association Equation of State (CPA-EoS) was used to model the experimental data.

##### **4-4-1 Cubic Plus Association Equation of state (CPA-EoS) model**

Based on classic thermodynamics, the following relation is valid for every component present in vapor-liquid-liquid equilibria:

$$f_i^v = f_i^{l,oleic} = f_i^{l,aqueous} \quad (4-1)$$

where  $f_i^v$ ,  $f_i^{l,oleic}$  and  $f_i^{l,aqueous}$  are the fugacity of component  $i$  in vapor phase, and hydrocarbon-rich and water-rich liquid phases, respectively. Fugacity is the corrected partial pressure of the component present in the mixture, and the fugacity of component  $i$  can be written as:

$$f_i = z_i \varphi_i P \quad (4-2)$$

where  $z_i$  and  $\varphi_i$  represent the mole fraction and fugacity coefficient of component  $i$ , respectively, and  $P$  represents the system pressure. The fugacity coefficient can be derived as follows:

$$\ln \varphi_i = \frac{1}{RT} \left( \frac{\partial A^r}{\partial n_i} \right)_{T,V,n_{j \neq i}} - \ln Z \quad (4-3)$$

The CPA-EoS model combines the SRK EoS model with an advanced association term based on Wertheim's theory to measure the polar/association effect of the mixture [25]. The mathematical expressions in equations (4) to (10) were used to develop the CPA-EoS model [26].

$$P = \frac{RT}{V_m - b} - \frac{a(T)}{V_m(V_m + b)} - \frac{1}{2} \frac{RT}{V_m} \left( 1 + \rho_m \frac{\partial \ln g}{\partial \rho_m} \right) \sum_i z_i \sum_{A_i} (1 - X_{A_i}) \quad (4-4)$$

where  $P$  is the pressure,  $a(T)$  is the energy parameter,  $b$  represents the co-volume term,  $R$  is the universal gas constant,  $V_m$  is the molar volume, and  $\rho_m$  is the molar density. The most crucial term in this equation is the association term  $X_{A_i}$ , which determines the self and cross-association of the component  $i$ .  $X_{A_i}$  can be represented using

$$X_{A_i} = \frac{1}{1 + \rho_m \sum_j z_j \sum_{B_j} X_{B_j} \Delta^{A_i, B_j}} \quad (4-5)$$

where  $Z_j$  is the mole-fraction of the molecule  $j$ ,  $\Delta^{A_i, B_j}$ , and is the association strength between site A of the molecule  $i$  and site B of the molecule  $j$ .

$$\Delta^{A_i, B_j} = g(\rho) \left[ \exp\left(\frac{\varepsilon^{A_i B_j}}{RT}\right) - 1 \right] b_{ij} \beta^{A_i B_j} \quad (4-6)$$

$$b_{ij} = \frac{b_i + b_j}{2} \quad (4-7)$$

where  $g$  is the radial distribution parameter,  $\varepsilon^{A_i B_j}$  &  $\beta^{A_i B_j}$  are the association energy and volume between site A on the molecule  $i$ , and site B on the molecule  $j$ , respectively.

$$a(T) = a_0 \left( 1 + m(1 - T_r^{0.5}) \right)^2 \quad (4-8)$$

$$g(\rho_m) = \frac{1}{1 - 1.9\eta} \quad (4-9)$$

$$\eta = \frac{1}{4} b \rho_m \quad (4-10)$$

#### **4-4-2 Models' parameters and data correlation**

To model the experimental vapor-liquid-liquid equilibria (VLLE) data, the CPA-EoS model was developed in MATLAB using a flash algorithm. The physical properties of the pure components were extracted from published literature. Although no asphaltene precipitation was observed at the operating conditions, the bitumen was considered as one pseudo-components that is a saturated-rich compound (PC1), and the second pseudo-component (PC2)

is asphaltene-rich. Furthermore, the second pseudo-component (PC2) has self-association with other PC2 and cross-association with PC1 [27–29]. Table 4-2 lists the pure components' critical properties and the CPA parameters for the associating and non-associating components.

Table 4-2: Model's parameter used in the VLE, LLE, and VLLE CPA EoS calculations.

Parameters	H <sub>2</sub> O	n-C <sub>6</sub>	PC1	PC2
$b$ (L/mol)	0.0145 [27] [25]	0.1078 [27]	0.4100 [25]	0.6300 [25]
$a_0$ (bar. L <sup>2</sup> /mol <sup>2</sup> )	1.2277 [27]	23.6810 [27]	409.77 [25]	1066.10 [25]
$c_1$	0.6736 [27]	0.83130 [27]	2.00 [25]	2.56 [25]
$\epsilon^{AB}$ (bar.L.mol <sup>-1</sup> )	166.55 [25]	-	-	249.42 [28]
$\beta^{AB}$	0.0692 [28]	-	-	0.05 [28]
$T_{cm}$	303.17 [25]	522.32 [25]	886.93 [23]	999.97 [25]

## **4-5 Results**

### **4-5-1 VLLE Experiments of the ternary system of normal-hexane, water and Mackay River bitumen**

Vapor-liquid-liquid equilibria (VLLE) study of the ternary system of normal-hexane, water and Mackay River bitumen mixture was performed at temperatures ranging from 185-210 °C and 2.5 MPa pressure. The concentration of n-C<sub>6</sub>/H<sub>2</sub>O was varied to understand the effect of solvent on the phase behavior and the thermophysical properties. In a typical SA-SAGD process, a solvent is normally co-injected with steam at low concentrations. In this work, two solvent mole fractions of 0.01 and 0.05 (6.85 and 27.7 vol.%) of water/hexane were considered. The mole fraction of hexane in a mixture of bitumen/solvent was maintained at 0.7 (37.45 vol.%), close to the maximum solubility of hexane in bitumen/solvent at the operational condition of solvent-aided thermal recovery processes of bitumen from oil sands. In addition to the VLLE phase equilibria study, the viscosity and density of the two observed liquid phases, the hydrocarbon-rich oleic liquid phase and water-rich aqueous phase were measured. The measured experimental data are reported in Table 4-3. Phase equilibria study of the ternary mixture of normal-hexane, water and Mackay River bitumen demonstrated a vapor-liquid-

liquid equilibrium (VLLE) at the temperature ranges from 191 to 211 °C and 2.5 MPa pressure; however, liquid-liquid equilibria (LLE) were observed at 185.6 °C and 2.5 MPa.

The results show that the vapor phase consists of n-C<sub>6</sub> and water. The concentration of n-C<sub>6</sub> in the vapor phase of the VLLE for the studied ternary mixture is compared with the vapor phase of binary n-C<sub>6</sub>/H<sub>2</sub>O system where the overall concentration of n-C<sub>6</sub> in the system is less than the azeotropic point concentration ( $y_{C_6}=0.6029$ ) [20] as shown in Figure 4-3. The results showed that the concentration of n-C<sub>6</sub> decreases with the increase in temperature, and the concentration of n-C<sub>6</sub> in the ternary system vapor phase is close to the binary n-C<sub>6</sub>/H<sub>2</sub>O system at the same pressure. These results suggest that the presence of bitumen does not significantly affect the solvent content of the vapor phase. The maximum standard deviation of the estimated n-C<sub>6</sub> concentration in vapor phase is 0.0178 (with an average standard deviation of 0.0142).

The mole fraction of n-C<sub>6</sub> and water present in the oleic phase are plotted in Figure 4-4. The results infer that the concentration of n-C<sub>6</sub> in the oleic phase decreases with the temperature increase, while the concentration of H<sub>2</sub>O increases with temperature. The average standard deviation of the estimated mole-fraction of n-C<sub>6</sub> and water in the oleic phase were 0.0238 and 0.0432, respectively. The K value of n-C<sub>6</sub> with respect to the mole-fraction of n-C<sub>6</sub> in the hydrocarbon-rich oleic phase ( $K_{C_6} = y_{C_6}^{vap} / y_{C_6}^{oleuc}$ ) were estimated at the studied temperature range and are plotted in Figure 4-5. The K value of n-C<sub>6</sub> shows a slight increase with temperature. The measured viscosity and density of the oleic phase over the studied temperature ranges are plotted in Figures 4-6 (a) and 4-7 (a), respectively. Figure 4-6(a) shows that the viscosity of the oleic phase increases with the increase in temperature, whereas bitumen viscosity reduces with the increase in temperature. This observation is related to the lower solubility of n-C<sub>6</sub> in bitumen at high temperatures. Solvent (n-C<sub>6</sub>) significantly impacts the mixture viscosity since its viscosity is very low compared with the bitumen. Figure 4-7(a and b) shows that the density measurements using the pycnometer. The density measurements are

highly prone to errors and only provide an approximate range of the density of the liquid phases over the temperature range of interest.

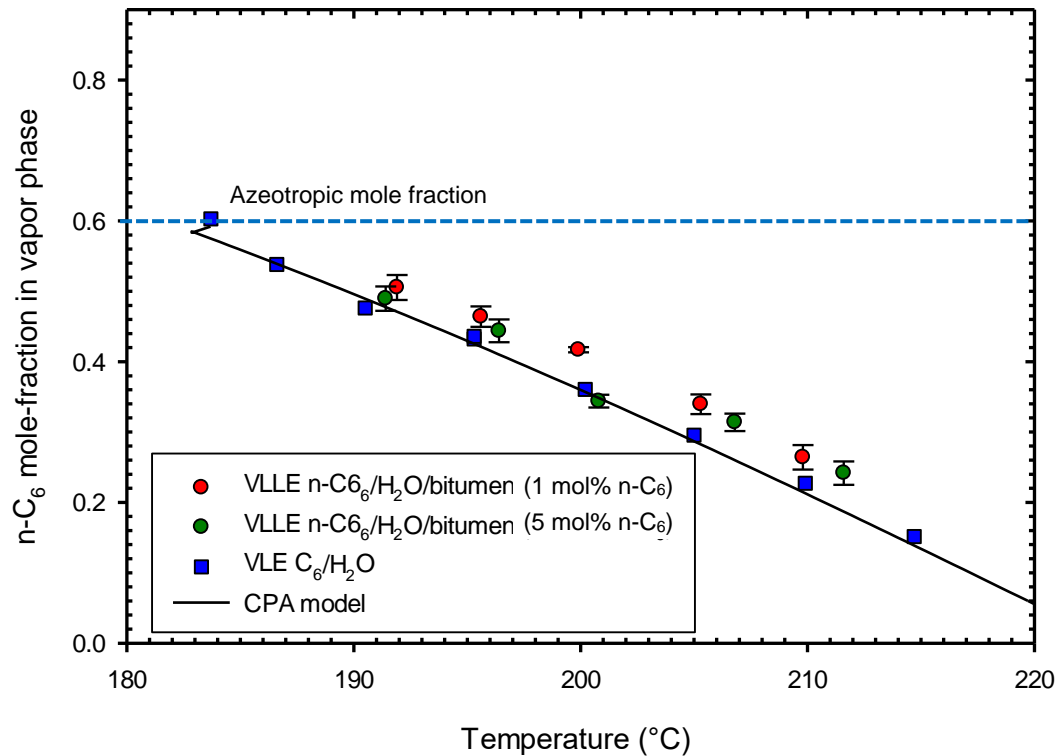


Figure 4-3: Comparison of the mole fraction of n-C<sub>6</sub> in the vapor phase of the ternary n-C<sub>6</sub>/H<sub>2</sub>O /Mackay River bitumen ternary system as compared with the n-C<sub>6</sub>/ H<sub>2</sub>O binary system [20] at the range of studied temperatures and 2.5 MPa pressure. Experimental data: rectangle (■) represents the binary mixture of n-C<sub>6</sub>/ H<sub>2</sub>O, and circles (●, red and ●, green) represent the ternary system (solvent/steam composition: ●, 1 mol. % n-C<sub>6</sub> (6.85 vol.%) and ●, 5 mol. % n-C<sub>6</sub> (27.7 vol.%). The mole fraction of hexane in a mixture of bitumen/solvent was maintained at 0.7 (37.45 vol.%)

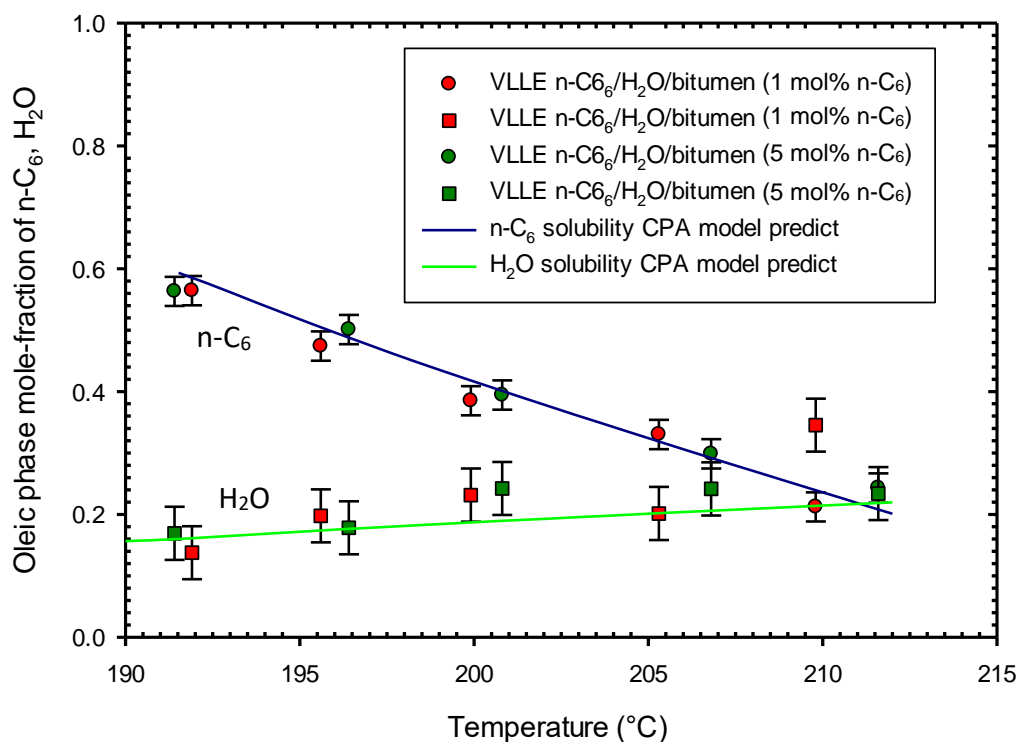


Figure 4-4: Solubilities of n-C<sub>6</sub> and H<sub>2</sub>O in the oleic phase. Experimental data: rectangles (■, red & ■, green) represent mole-fraction of H<sub>2</sub>O, and circles (●, red & ●, green) represent mole-fraction of n-C<sub>6</sub> (red, 6.85 LVE% of n-C<sub>6</sub> and green, 27.7 LVE% of n-C<sub>6</sub>). Model: solid line represents the CPA-EoS model predicted mole fraction. Solvent/steam composition: ●, 1 mol. % n-C<sub>6</sub> (6.85 vol.%) and ●, 5 mol. % n-C<sub>6</sub> (27.7 vol.%). The mole fraction of hexane in a mixture of bitumen/solvent was maintained at 0.7 (37.45 vol.%).

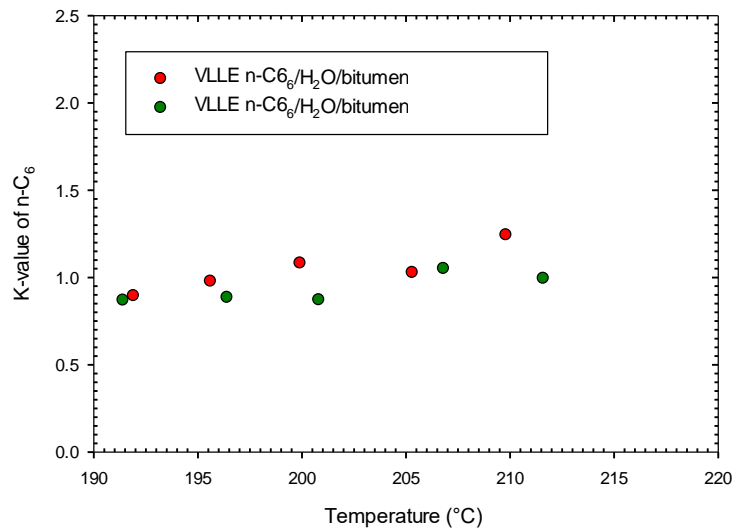


Figure 4-5: K value of n-C<sub>6</sub> with respect to the mole-fraction of n-C<sub>6</sub> in the hydrocarbon-rich oleic phase. ( $K_{C_6} = y_{C_6}^{vap} / y_{C_6}^{oleuc}$ ). Experimental data: ●, 6.85 LVE% of n-C<sub>6</sub> and ●, 27.7 LVE% of n-C<sub>6</sub>. (solvent/steam composition: ●, 1 mol. % n-C<sub>6</sub> (6.85 vol.%) and ●, 5 mol. % n-C<sub>6</sub> (27.7 vol.%). The mole fraction of hexane in a mixture of bitumen/solvent was maintained at 0.7 (37.45 vol.%).

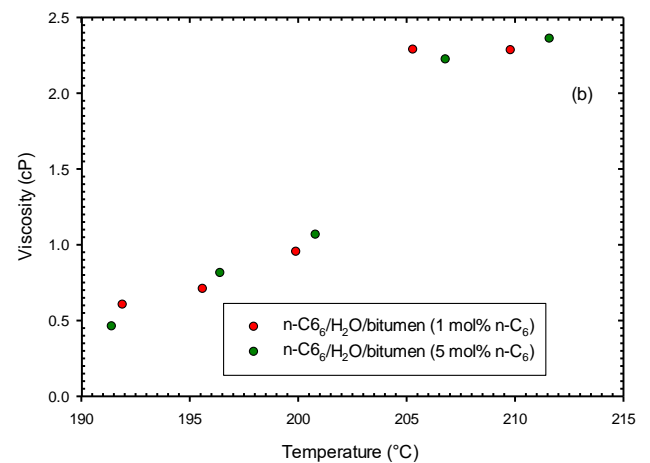
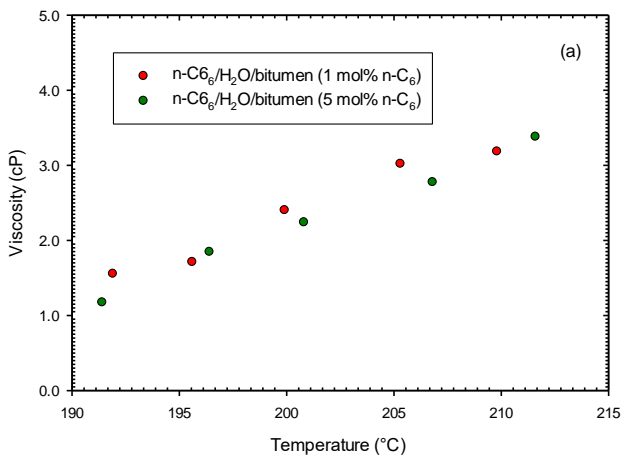


Figure 4-6: (a) Viscosity of the hydrocarbon-rich oleic phase. (b) Viscosity of the water-rich aqueous phase. Experimental data: ●, 6.85 LVE% of n-C<sub>6</sub>, ●, 27.7 LVE% of n-C<sub>6</sub>. Solvent/steam composition: ●, 1 mol. % n-C<sub>6</sub> (6.85 vol.%) and ●, 5 mol. % n-C<sub>6</sub> (27.7 vol.%)

. The mole fraction of hexane in a mixture of bitumen/solvent was maintained at 0.7 (37.45 vol.%).

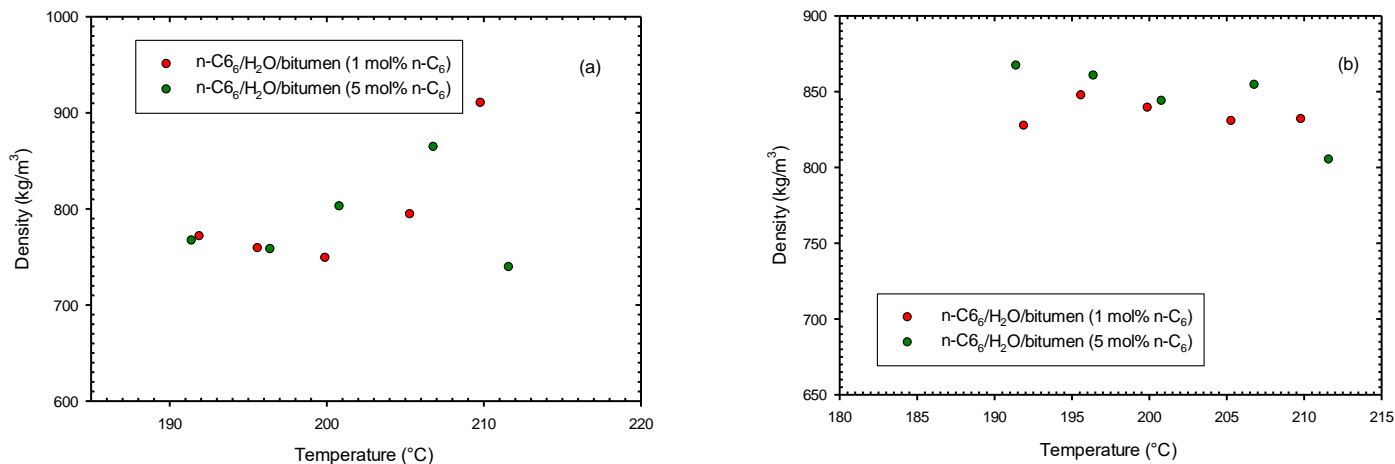


Figure 4-7: (a) The density of the hydrocarbon-rich oleic phase. (b) The density of the water-rich aqueous phase. Experimental data: ●, 6.85 LVE% of n-C<sub>6</sub>, ●, 27.7 LVE% of n-C<sub>6</sub>. Model: solid line represents the CPA-EoS model predicted density. Solvent/steam composition: ●, 1 mol. % n-C<sub>6</sub> (6.85 vol.%) and ●, 5 mol. % n-C<sub>6</sub> (27.7 vol.%) . The mole fraction of hexane in a mixture of bitumen/solvent was maintained at 0.7 (37.45 vol.%).

Water with a trace amount of n-C<sub>6</sub> was observed in the water-rich aqueous phase. The results show that the solubility of n-C<sub>6</sub> in the aqueous phase of the ternary n-C<sub>6</sub>/H<sub>2</sub>O/bitumen system (VLLE) is very close to the one in the binary n-C<sub>6</sub>/H<sub>2</sub>O binary system (VLE) [20]. The presence of hydrocarbon and inorganic components in the water-rich aqueous phase was also tested. The result showed that 18.2 mg /L of hydrocarbon components and 86 mg/L of total dissolved solid were present in the aqueous phase. The mole fraction of n-C<sub>6</sub> and water in the aqueous phase are plotted against the temperature range in Figure 4-8. The results don't show a significant trend for the mole fraction of n-C<sub>6</sub> and H<sub>2</sub>O. The inset plot in Figure 4.8 shows the collected water samples. The maximum standard deviation of the estimated mole-fraction of n-C<sub>6</sub> in the aqueous phase is 0.0002.

The measured viscosity and density of the aqueous phase are plotted against the temperature ranges in Figures 4-6b and 4-7b, respectively. Figure 4-6b shows that the viscosity of the aqueous phase increases with temperature, whereas pure water demonstrates decreasing trend. The presence of hydrocarbon components and total dissolved solid in the aqueous phase may have impact on the viscosity of the aqueous phase. Figure 4-7b shows the approximate range of the density of the aqueous phase over the studied temperature range.

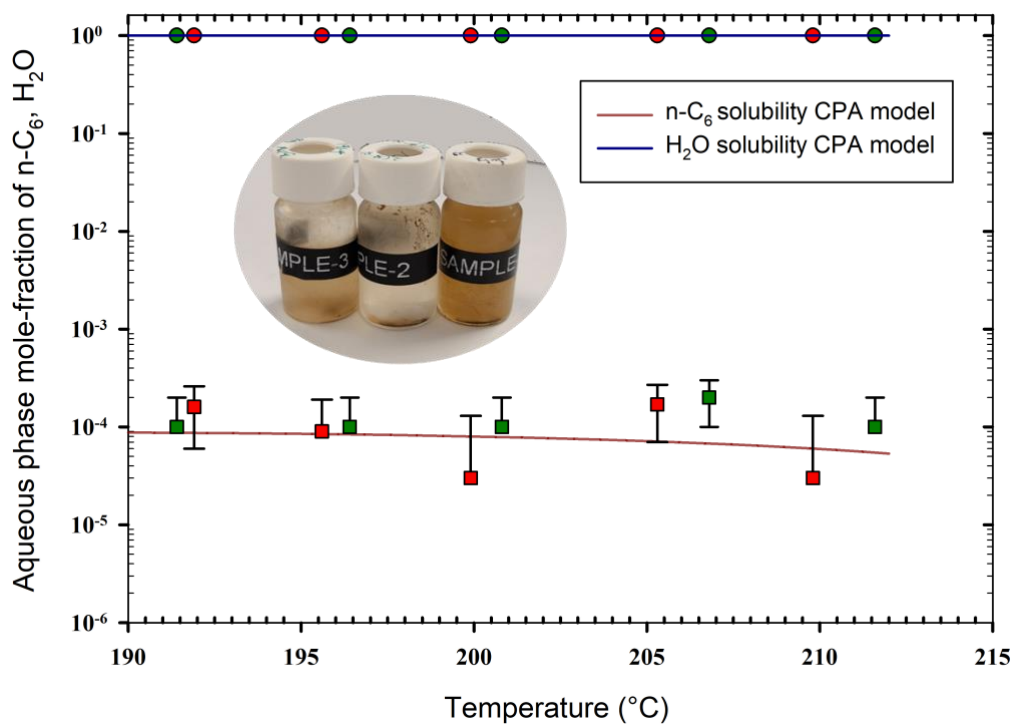


Figure 4-8: Solubilities of n-C<sub>6</sub> and H<sub>2</sub>O in the aqueous phase. Experimental data: rectangles (■, red & ■, green) represent mole-fraction of n-C<sub>6</sub>, and circles (●, red & ●, green) represent mole-fraction of H<sub>2</sub>O. Solvent/steam composition: ●, 1 mol. % n-C<sub>6</sub> (6.85 vol.%) and ●, 5 mol. % n-C<sub>6</sub> (27.7 vol.%). The mole fraction of hexane in a mixture of bitumen/solvent was maintained at 0.7 (37.45 vol.%).

#### **4.5.2 VLLE modeling of the ternary system of normal-hexane, water and Mackay River bitumen**

CPA EoS was used to model the multiphase equilibria, and the results are compared with the experimental solubilities of n-C<sub>6</sub> and water in the vapor, oleic and aqueous phases. Table 4-2 shows the CPA EoS parameters obtained from VLE data and was directly used without further tuning. The parameters for modeling the interaction between water and bitumen are listed in Table 4-4 [30]. The cross-association, binary interaction parameters between bitumen pseudo-components, and the molecular weight of PC2 are presented in Table 4-5 [30]. These parameters are also used directly without further tuning. The tuned binary interaction parameter of n-C<sub>6</sub> and bitumen are presented in Table 4-6.

The results shown in Figure 4-3 reveal that the CPA EoS predictions of vapor phase composition of the binary mixture of n-C<sub>6</sub>/water are acceptable, with an overall RSME of 0.0234 %. However, those of the ternary system of n-C<sub>6</sub>/water/bitumen are far from the experimental observations. The normal hexane and water solubilities in the oleic and aqueous phases predicted with the CPA model are plotted in Figures 4-4 and 4-8, respectively. The root mean error (RMSE) n-C<sub>6</sub> and water solubilities in the oleic phase were found to be 0.07 and 0.17, respectively. For the aqueous phase, the solubility data was modeled assuming that there is no bitumen dissolved in the aqueous phase. The model predicted the n-C<sub>6</sub> solubility in the aqueous phase with an RMSD of  $2.04 \times 10^{-4}$ . The density of the oleic phase was also predicted with the CPA model and compared in Figure 4-7(a).

Table 4-3: Phase behavior, viscosity, and density data for VLLE of the ternary n-C<sub>6</sub>/H<sub>2</sub>O /bitumen system.

Temperature (°C)	Pressure (MPa)	System	Vapor phase <sup>a</sup>		Oleic phase <sup>b</sup>			Aqueous phase <sup>c</sup>		
			Mole fraction of C <sub>6</sub> (y <sub>C<sub>6</sub></sub> )	Mole fraction of C <sub>6</sub> (x <sub>C<sub>6</sub></sub> )	Mole- fraction of H <sub>2</sub> O (x <sub>H<sub>2</sub>O</sub> )	Viscosity (cP)	Density (kg/m <sup>3</sup> )	Mole-fraction of C <sub>6</sub> (x <sub>C<sub>6</sub></sub> )	Viscosity (cP)	Density (kg/m <sup>3</sup> )
Solvent/steam composition: 1 mol. % n-C <sub>6</sub> (6.85 vol.%) in n-C <sub>6</sub> /H <sub>2</sub> O mixture. The mole fraction of hexane in a mixture of bitumen/solvent was maintained at 0.7 (37.45 vol.%).										
185.6	2.50	LLE	-	0.6070	0.1131	1.31	765.0	0.0002	0.41	864.0
191.9	2.52	VLLE	0.5055	0.5645	0.1375	1.56	771.6	0.0002	0.60	827.6
195.6	2.51	VLLE	0.4638	0.4742	0.1976	1.71	759.0	0.0001	0.71	848.0
199.9	2.55	VLLE	0.4171	0.3850	0.2314	2.40	749.0	0.0000	0.95	839.0
205.3	2.54	VLLE	0.3394	0.3301	0.2014	3.02	794.5	0.0002	2.29	830.6
209.8	2.53	VLLE	0.2640	0.2121	0.3453	3.19	910.5	0.0000	2.28	832.0
Solvent/steam composition: 5 mol. % n-C <sub>6</sub> (27.7 vol.%) in n-C <sub>6</sub> /H <sub>2</sub> O mixture. The mole fraction of hexane in a mixture of bitumen/solvent was maintained at 0.7 (37.45 vol.%).										
191.4	2.52	VLLE	0.4897	0.5632	0.1691	1.17	767.0	0.0001	0.46	867.3
196.4	2.52	VLLE	0.4438	0.5012	0.1782	1.85	758.0	0.0001	0.81	860.7
200.8	2.57	VLLE	0.3438	0.3942	0.2422	2.24	803.0	0.0001	1.07	844.0
206.8	2.51	VLLE	0.3137	0.2985	0.2414	2.78	864.5	0.0002	2.22	854.5
211.6	2.51	VLLE	0.2416	0.2429	0.2338	3.38	739.3	0.0001	2.36	805.2

<sup>a</sup>: Vapor phase:  $y_{C_6} + y_{H_2O} = 1$   
<sup>b</sup>: Oleic phase:  $x_{C_6} + x_{H_2O} + x_{bitumen} = 1$   
<sup>c</sup>: Oleic phase:  $x_{C_6} + x_{H_2O} = 1$

Table 4-4 Cross-association and binary interaction parameters between water and bitumen pseudo-components [30]

Parameter	$\epsilon^{\text{PC2,w}}/R$ (K)	$K^{\text{PC1,w}}$	$K^{\text{PC2,w}}$
Value	$2484.57 + 0.01T$	$9.25 \times 10^{-4} + 4.51 \times 10^{-3}T$	$0.66 - 7.56 \times 10^{-5}T$

Table 4-5: Bitumen parameters [30]

Parameter	$\epsilon^{\text{PC2,PC1}}/R$ (K)	$K^{\text{PC1,PC2}}$	$MW_{\text{PC2}}$ (g/mol)
Value	$2035.61 + 0.22T$	$0.04 + 8.53 \times 10^{-5}T$	$790.26 - 0.41T$

Table 4-6: Binary interaction parameters between n-C<sub>6</sub> and bitumen pseudo-components

Solvent	$K^{\text{PC1,solvent}}$	$K^{\text{PC2,solvent}}$	RMSD
n-C <sub>6</sub>	$0.29 - 4.26 \times 10^{-3}T$	$0.86 + 7.83 \times 10^{-4}T$	0.05

#### **4-6 Summary and Conclusions**

Phase behavior study of the ternary mixture of n-C<sub>6</sub>, H<sub>2</sub>O and bitumen were performed at the temperature's ranges from 190-210 °C and 2.5 MPa pressure. In a typical SA-SAGD process, a solvent is normally co-injected with steam at low concentrations. In this work, we considered two solvent mole fractions of 0.01 and 0.05 (6.85 and 27.7 vol.%) of water/hexane. The mole fraction of hexane in a mixture of bitumen/solvent was maintained at 0.7 (37.45 vol.%), near the maximum solubility of hexane in bitumen/solvent at the operational condition of solvent-aided thermal recovery processes of bitumen from oil sands. The VLLE phase equilibrium of n-C<sub>6</sub>/water/bitumen is studied, and the viscosity and density of the liquid phases, hydrocarbon-rich oleic liquid phase and water-rich aqueous phase were measured. The CPA EoS was used to model the measured multiphase equilibrium data, and the results are compared with the experimental solubilities of n-C<sub>6</sub> and water in the vapor, oleic and aqueous phases. The results reveal that at VLLE conditions studied, the solvent concentration co-injected with steam does not affect phase equilibrium and thermophysical properties of phases. Furthermore, the results indicate that the mole-fraction of the n-C<sub>6</sub> present in the vapor phase is close to the binary mixture of n-C<sub>6</sub>/H<sub>2</sub>O, and the concentration of n-C<sub>6</sub> decreases in the vapor phase with the increase in temperature. Finally, our findings suggest that the presence of bitumen does not have a significant effect on the steam solvent condensation behavior. Therefore, the binary solvent/water systems may be used for condensation studies of SA-SAGD .

#### **4-7 Reference**

- [1] T.N. Nasr, G. Heck, H. Golbeck, G. Beaulieu, Novel Expanding Solvent-SAGD Process ES-SAGD, *Journal of Canadian Petroleum Technology*. 42 (2003).
- [2] L.M. Dittaro, A.E. Jaafar, D.L. Perlau, T.J. Boone, J.A. Yerian, J.L. Dickson, R. C. Wattenbarger, A.E. Jaafar, Findings from a Solvent-Assisted SAGD Pilot at Cold Lake, in: Paper Presented at the SPE Heavy Oil Conference-Canada, Calgary, Alberta, Canada, 2013.
- [3] S.C. Gupta, S.D. Gittins, Christina Lake Solvent Aided Process Pilot, *Journal of Canadian Petroleum Technology*. 45 (2006).
- [4] H. Nourozieh, M. Kariznovi, J. Abedi, Phase Behavior Study of Butane / Athabasca Bitumen Mixtures Applicable for Thermal and Hybrid Solvent Recovery Processes, in: Paper Presented at SPE Heavy Oil Conference-Canada, Calgary, 2014.
- [5] A. Memarzadeh, H. Rahnema, Thermodynamic Analysis of Solvent Assisted Steam Injection., in: Paper Presented at the SPE Annual Technical Conference and Exhibition, Houston, Texas, USA, Houston, Texas, USA, 2015.
- [6] H.S. Yamchi, M. Zirrahi, H. Hassanzadeh, J. Abedi, Measurements and NRTL modeling of liquid-liquid equilibrium of dimethyl ether/bitumen, *Fluid Phase Equilib*. 512 (2020).
- [7] K. Sheng, R. Okuno, A. Al-Gawfi, P. Nakutnyy, M. Imran, K. Nakagawa, An Experimental Study of Steam-Solvent Coinjection for Bitumen Recovery Using a Large-Scale Physical Model, *SPE Journal*. 27 (2022) 381–398. <https://doi.org/10.2118/205158-PA>.
- [8] N. Sabet, H. Hassanzadeh, J. Abedi, Selection of efficient solvent in solvent-aided thermal recovery of bitumen, *Chem Eng Sci*. 161 (2017) 198–205. <https://doi.org/https://doi.org/10.1016/j.ces.2016.12.031>.
- [9] S.M. Jafari Raad, H. Hassanzadeh, Subsurface Containment of Injected Chemicals during In-Situ Bitumen Recovery from Oil Sands, *ACS ES&T Engineering*. 2 (2022) 681–688. <https://doi.org/10.1021/acsestengg.1c00358>.

- [10] C.T. Fu, V.R. Puttagunta, G. Vilcsak, Gas Solubility Of Methane And Ethane In Cold Lake Bitumen At In Situ Conditions, *Journal of Canadian Petroleum Technology*. 27 (1988). <https://doi.org/10.2118/88-04-06>.
- [11] H. Nourozieh, M. Kariznovi, J. Abedi, Experimental and modeling studies of phase behavior for propane/Athabasca bitumen mixtures, *Fluid Phase Equilib.* 397 (2015) 37–43. <https://doi.org/https://doi.org/10.1016/j.fluid.2015.03.047>.
- [12] Y. Dini, M. Becerra, J.M. Shaw, Phase Behavior and Thermophysical Properties of Peace River Bitumen + Propane Mixtures from 303 K to 393 K, *J Chem Eng Data*. 61 (2016) 2659–2668. <https://doi.org/10.1021/acs.jced.6b00034>.
- [13] M. Zirrahi, H. Hassanzadeh, J. Abedi, Experimental and modeling studies of water, light n-alkanes and MacKay River bitumen ternary systems, *Fuel*. 196 (2017) 1–12. <https://doi.org/https://doi.org/10.1016/j.fuel.2017.01.078>.
- [14] A. Haddadnia, H. Sadeghi Yamchi, M. Zirrahi, H. Hassanzadeh, J. Abedi, New Solubility and Viscosity Measurements for Methane–, Ethane–, Propane–, and Butane–Athabasca Bitumen Systems at High Temperatures up to 260 °C, *J Chem Eng Data*. 63 (2018) 3566–3571. <https://doi.org/10.1021/acs.jced.8b00443>.
- [15] A. Haddadnia, M. Zirrahi, H. Hassanzadeh, J. Abedi, Thermo-Physical Properties of n-Pentane/Bitumen and n-Hexane/Bitumen Mixtures Systems, *Can J Chem Eng*. 96 (2017). <https://doi.org/10.1002/cjce.22873>.
- [16] H. Sadeghi Yamchi, M. Zirrahi, H. Hassanzadeh, J. Abedi, H. Fadaei, Effect of additives on liquid–liquid equilibrium properties of butane/bitumen systems with applications to solvent aided bitumen recovery processes, *Chemical Engineering Research and Design*. 137 (2018) 452–460. <https://doi.org/https://doi.org/10.1016/j.cherd.2018.08.007>.

- [17] A. Haddadnia, B. Azinfar, M. Zirrahi, H. Hassanzadeh, J. Abedi, Thermophysical Properties of Dimethyl Ether/Athabasca Bitumen System, *Can J Chem Eng.* 96 (2017). <https://doi.org/10.1002/cjce.23009>.
- [18] H. Sadeghi Yamchi, M. Zirrahi, H. Hassanzadeh, J. Abedi, Measurements and NRTL modeling of liquid-liquid equilibrium of dimethyl ether/bitumen, *Fluid Phase Equilib.* 512 (2020) 112549. <https://doi.org/10.1016/j.fluid.2020.112549>.
- [19] M. bin Dahbag, M. Zirrahi, H. Hassanzadeh, Solubility and Liquid Density of Ammonia/Athabasca Bitumen Mixtures at Temperatures up to 463 K: Measurements and Modeling, *J Chem Eng Data.* 64 (2019) 3592–3597. <https://doi.org/10.1021/acs.jced.9b00356>.
- [20] B. Azinfar, A. Haddadnia, M. Zirrahi, H. Hassanzadeh, J. Abedi, A thermodynamic model to predict propane solubility in bitumen and heavy oil based on experimental fractionation and characterization, *J Pet Sci Eng.* 168 (2018) 156–177. <https://doi.org/10.1016/j.petrol.2018.04.065>.
- [21] M. Zirrahi, H. Hassanzadeh, J. Abedi, Experimental and modeling studies of MacKay River bitumen and water, *J Pet Sci Eng.* 151 (2017) 305–310. <https://doi.org/10.1016/j.petrol.2017.01.013>.
- [22] B. Azinfar, M. Zirrahi, H. Hassanzadeh, J. Abedi, Characterization of heavy crude oils and residues using combined Gel Permeation Chromatography and simulated distillation, *Fuel.* 233 (2018) 885–893. <https://doi.org/10.1016/j.fuel.2018.06.110>.
- [23] A. Karevan, M. Zirrahi, H. Hassanzadeh, Standardized High-Performance Liquid Chromatography to Replace Conventional Methods for Determination of Saturate, Aromatic, Resin, and Asphaltene (SARA) Fractions, *ACS Omega.* 7 (2022) 18897–18903. <https://doi.org/10.1021/acsomega.2c01880>.

- [24] C. Nwokoye, D. Nath, M. Abdi, M. Khalifi, H. Hassanzadeh, Vapor-liquid Equilibria (VLE) of the binary mixture of normal hexane and water at  $P = 2.5$  MPa and  $T=(456.85-487.85$  K), Submitted for Publication. (2022).
- [25] M. Abdi, H.S. Yamchi, M. Zirrahi, H. Hassanzadeh, Cubic-plus-association equation of state parameterization of liquid-liquid equilibrium of propane + n-butane + bitumen and dimethyl ether + bitumen systems, *Fluid Phase Equilib.* 554 (2022) 113341. <https://doi.org/https://doi.org/10.1016/j.fluid.2021.113341>.
- [26] M.L. Michelsen, E.M. Hendriks, Physical properties from association models, *Fluid Phase Equilib.* 180 (2001) 165–174. [https://doi.org/https://doi.org/10.1016/S0378-3812\(01\)00344-2](https://doi.org/https://doi.org/10.1016/S0378-3812(01)00344-2).
- [27] G.M. Kontogeorgis, M.L. Michelsen, G.K. Folas, S. Derawi, N. von Solms, E.H. Stenby, Ten Years with the CPA (Cubic-Plus-Association) Equation of State. Part 1. Pure Compounds and Self-Associating Systems, *Ind Eng Chem Res.* 45 (2006) 4855–4868. <https://doi.org/10.1021/ie051305v>.
- [28] J Mauk Smith, Hendrick C. Van Ness, Michael M. Abbott, Mark Thomas Swihart, Introduction to Chemical Engineering Thermodynamics, American Chemical Society, 1950.
- [29] H. Sadeghi Yamchi, M. Zirrahi, H. Hassanzadeh, J. Abedi, Measurements and modeling of liquid-liquid equilibrium of Propane + n-Butane + Bitumen system, *Fuel.* 293 (2021) 120353. <https://doi.org/https://doi.org/10.1016/j.fuel.2021.120353>.
- [30] M. Abdi, M. Zirrahi, H. Hassanzadeh, Vapor–Liquid–Liquid Equilibrium Modeling of Water/Bitumen/Solvent ( $C_1$ ,  $C_2$ ,  $C_3$ , and n- $C_4$ ) Mixtures Using a Cubic-Plus-Association Equation of State, *Ind Eng Chem Res.* 61 (2022) 8279–8292. <https://doi.org/10.1021/acs.iecr.2c00873>.

## **Chapter 5: Conclusions and Recommendations**

### **5-1 Summary**

The present interest in solvent-aided techniques like ES-SAGD, N-SOLV, ESEIEH, and LASER is a result of the rise in demand for more environmentally friendly, reliable, and cost-effective methods of bitumen recovery. In these processes, a solvent and steam mixture are injected into oil sands reservoirs to dissolve the solvent into bitumen, speeding up the viscosity reduction, lowering the steam consumption and, consequently, lowering the SOR. The full-scale implementation of these technologies has been partly hindered by the knowledge gap in understanding the complex phase behavior of solvent/steam/bitumen mixtures.

Numerous numerical simulations and experimental studies have been carried out to better understand the process and the associated phase behavior. The focus of simulation and numerical studies has been on optimizing solvent concentration, selecting the best solvent type, and understanding the behavior of the steam/solvent chamber in the presence and absence of barriers. The experimental measurements have been conducted to understand phase equilibria better and measure the thermophysical properties of solvent/bitumen/water systems.

In this thesis, the phase equilibria of binary normal hexane/water and ternary normal hexane/water/bitumen mixtures at temperatures ranging from 180-215 °C and 2.5 MPa pressure are studied to understand the condensation behavior and related thermophysical properties.

### **5-2 Conclusions**

The results indicated an azeotropic behavior for the normal hexane/water binary system. The azeotropic behavior occurred at a hexane mole fraction of ~0.6029 of normal hexane at ~183.7 °C. Below the azeotropic temperature, a liquid-liquid equilibrium (LLE) will occur. At solvent concentrations below the azeotrope mole fraction, the condensed phase is primarily water until the azeotropic point, when hexane begins to co-condense. On the other

hand, at solvent concentrations above the azeotrope mole fraction, the condensed phase is primarily hexane. The solubility of normal hexane in the water phase was found to be negligible. The cubic-plus-association equation of state (CPA EoS) and the nonrandom two-liquid (NRTL) model were used to correlate the measured data. The model predictions are in good agreement with the experimentally measured values.

The second experimental task was conducted to study the phase equilibria of the hexane/ water/Mackay River bitumen ternary system and measure the viscosity and density of the associated liquid phases. VLLE was observed at temperatures ranging from 180-215 °C and 2.5 MPa. The amount of normal hexane in the vapor phase increased with temperature. The vapor phase for the ternary mixture was found to have a similar n-C<sub>6</sub> concentration when compared to n-C<sub>6</sub>/ H<sub>2</sub>O binary mixture. The findings reveal that the binary solvent/water equilibria may be used for condensation studies of SA-SAGS. The results also reveal that at VLLE conditions studied, the solvent concentration co-injected with steam does not affect phase equilibrium and thermophysical properties of phases.

### **5-3 Recommendations**

The measurements of phase behavior, viscosity, and density were carried out successfully using the experimental apparatus shown in the methodologies of Chapter 3 and Chapter 4. However, density measurement using a device capable of withstanding high temperature ( $T > 190^{\circ}\text{C}$ ) and pressure conditions is recommended to improve the results of density measurements.

Another suggestion is to perform experiments with different solvents (i.e., n-butane, diluents, gas condensates) to compare the condensation behavior with the n-hexane/water binary mixtures. Furthermore, VLLE studies using solvent additives may provide insight into solvent selection and controlling steam/solvent condensation in SA-SAGD processes, leading to more efficient in-situ bitumen recovery performance. Finally, investigating the effect of the

solvent/bitumen injection ratio would aid in understanding phase behavior and the effect of solvent on bitumen viscosity.